Am J Cancer Res 2022;12(1):337-354
www.ajcr.us /ISSN:2156-6976/ajcr0140925

Original Article

Exploiting induced vulnerability to overcome PARPi resistance and clonal heterogeneity in BRCA mutant triple-negative inflammatory breast cancer

David J H Shih[1,4], Mei-Kuang Chen[2], Jun Yin[6], Daniel J McGrail[1], Hui Dai[1], Rongbin Wei[1], Jing Zhang[1], Wenjin Jim Zheng[4], Kim-Anh Do[3], Liuqing Yang[2], Mien-Chie Hung[5], Shiaw-Yih Lin[1]

Departments of [1]Systems Biology, [2]Molecular and Cellular Oncology, [3]Biostatistics, University of Texas MD Anderson Cancer Center, Houston, TX 77030-4009, USA; [4]School of Biomedical Informatics, University of Texas Health Science Center at Houston, Houston, TX 77030, USA; [5]China Medical University, Taichung 406040, Taiwan; [6]Caris Life Sciences, Irving, TX 75039, USA

Received December 2, 2021; Accepted December 27, 2021; Epub January 15, 2022; Published January 30, 2022

Abstract: Acquired resistance and clonal heterogeneity are critical challenges in cancer treatment, and the lack of effective computational tools hampers the discovery of new treatments to overcome resistance. Using high-throughput transcriptomic databases of compound perturbation profiles, we have developed a bioinformatic strategy for identifying candidate drugs to overcome resistance with combinatorial therapy. We devised this strategy during an investigation into the acquired resistance against PARP inhibitors (PARPi) in a triple-negative inflammatory breast cancer cell line. In this study, we derived multiple PARPi-resistant clones and characterized their transcriptomic adaptations compared to the parental clone. The transcriptomes of the resistant clones showed substantial heterogeneity, highlighting the importance of characterizing multiple clones from the same tumour. Surprisingly, we found that these transcriptomic changes may not actually confer PARPi resistance, but they may nevertheless induce a shared secondary vulnerability. By modeling our data in relation to transcriptomic perturbation profiles of compounds, we uncovered deficiencies in Ras signaling that resulted from transcriptional adaptation to long-term PARPi treatment across multiple resistant clones. Due to these induced deficiencies, we predicted that the resistant clones would be sensitive to pharmacological reinforcement of PARPi-induced transcriptional adaptation. We then experimentally validated this predicted vulnerability that is shared by multiple resistant clones. Our results thus provide a promising paradigm for integrating transcriptomic data with compound perturbation profiles in order to identify drugs that can exploit an induced vulnerability and overcome therapeutic resistance, thus providing another strategy towards precision oncology.

Keywords: PARP inhibitor resistance, triple-negative inflammatory breast cancer, clonal heterogeneity, transcriptomics, pharmacogenomics

Introduction

Acquired resistance to therapeutic treatment is a frequent challenge in cancer, and finding new treatments to overcome therapeutic resistance can be both difficult and time-consuming. Clonal heterogeneity further complicates the problem, since the treatment would ideally eradicate all cancer clones in order to minimize the chance of additional acquired resistance. Therefore, an efficient way of identifying novel candidates to combat resistance would help fuel the therapeutic development and thus improve clinical outcome. Here, we have developed a bioinformatic strategy that uses high-throughput transcriptomic databases of compound perturbation profiles in order to identify new treatments to overcome acquired resistance, and this bioinformatic development was motivated and informed by our study on resistance against PARP inhibitors.

PARP inhibitors (PARPi) are a class of drugs that target DNA damage repair, including olaparib, talazoparib, rucaparib, niraparib, as well as many other new drugs that show PARPi activity [1, 2]. These drugs have been shown to be effective against germline *BRCA1/2* mutant

triple-negative breast cancer, advanced ovarian cancer, metastatic pancreatic cancer, and metastatic prostate cancer [3-9]. Typically, PARPi exert their anti-cancer effects by trapping the PARP protein to the DNA, leading ultimately to DNA double-strand breaks and cell death [1, 10-12]. Now that PARPi are indicated for maintenance therapy lasting up to two years [3, 4, 6, 8], acquired resistance against PARPi represents a critical cause of treatment failure. We therefore seek to identify drugs that can be used in combination with PARPi in order to overcome resistance.

Here, we developed a new bioinformatic strategy to identify drugs to combat acquired resistance, by integrating high-throughput transcriptomic databases of compound perturbation profiles with transcriptomic characterization of resistant cancer clones. Currently, proteomic and transcriptomic profiling approaches are commonly used to discover candidates for combinatorial therapy, and candidates are often identified by short-term (48-96 hours) treatment of the primary drug and searching for secondary drugs that suppress activated pathways [13, 14]. These candidate drugs would then be commonly used in concurrent combination with the primary drug [1, 2, 15-20]. In contrast, we investigated resistance here in the context of long-term (10 months) treatment of the primary drug for the purpose of identifying promising therapeutic strategies to overcome resistance. Because clonal heterogeneity represents an important challenge, we characterized several resistant clones in order to identify shared vulnerabilities. We chose to focus on triple-negative inflammatory breast cancer, because it is the most lethal subtype of breast cancer [21]. After deriving PARPi-resistant cancer clones [22], we initially followed the above approach of suppressing pathways activated by PARPi in order to identify candidates for concurrent combinatorial treatment with PARPi. However, we then discovered that the mechanism of PARPi resistance was caused by a revertant *BRCA1* mutation. We thus revised our bioinformatic strategy to identify drugs that target secondary vulnerabilities induced by transcriptional adaptation to long-term PARPi treatment. Importantly, we validated our bioinformatic strategy by experimentally confirming the predicted vulnerability in the PARPi-resistant clones.

Materials and methods

Cell culture

The SUM149 cell line was maintained in Ham's F12K medium (ATCC, 30-2004) with 5% FBS, 10 mM HEPES, 1 μg/mL hydrocortisone, and 5 μg/mL insulin. PARPi-resistant clones were derived by long-term treatment with 50-100 nM talazoparib. Initially, cells were treated with 100 nM talazoparib with the medium replaced daily for 5 days, followed by 2 more days in 50 nM to allow apoptosis to complete. Single clones were trypsinized, picked, placed in 96-well plates for monoclonal expansion in 50 nM talazoparib, which took about 8 months (untreated SUM149 typically takes 8-10 weeks for monoclonal expansion). Subsequently, the clones were cultured in 25 nM talazoparib for the first 3 passages, and talazoparib treatment was discontinued after the cells began to stably proliferate (2-3 months). The clones were confirmed to be stably resistant to talazoparib, olaparib, and rucaparib even at high passage numbers.

Transcriptomic analysis

The SUM149 parental and PARPi-resistant clones were treated with 0.1% DMSO or 50 nM talazoparib for 48 hours in 3 biological replicates before total RNA was harvested with the Qiagen RNeasy kit (#74134) and submitted for whole transcriptome sequencing (2×76 bp paired-end) at the MD Anderson Sequencing and Microarray Facility. About 20-30 million read pairs were generated per sample, with an average insert size of 200 bp. Across 51 samples, about 93-94% of reads had base quality ≥30, and the mean base quality scores were 38-39.

Quality assessment of reads was determined by FastQC (v0.11.3), which detected minor adapter contamination. Therefore, contaminating adapters were removed using cutadapt [23] (v1.17). Transcript expression was quantified directly without alignment using salmon with bias correction [24] (v0.11.2). Batch effects were estimated using ComBat as implemented in sva [25] (v3.32.1). Differential expression Wald statistics were estimated using DESeq2 [25, 26] (v1.24.0). Gene set enrichment scores were calculated with GSVA [27] (v.1.32.0). Competitive gene set enrichment analysis was

performed using CAMERA [28] as implemented in limma [29] (v3.40.2). Gene sets were acquired from the Molecular Signatures Database [30-32] (MSigDB v6.2). Expression data from the TCGA were retrieved from the Genomic Data Commons. Triple negative breast cancer (basal subtype) samples in the TCGA were identified by the PAM50 classifier as implemented in genefu [33] (v2.16.0). Plots were generated using ggplot2 [34] (v3.3.2) and ComplexHeatmaps [35] (v2.0.0). To investigate the *BRCA1* locus, read pairs were aligned using STAR [36] (v2.7.2b) and visualized using the Integrative Genomics Viewer [37] (v2.4.18) with soft-clipped bases visible. Potentially misaligned reads were re-aligned using BLAT.

Integrative analysis with perturbation maps

Broad Connectivity Map (CMap) Phase 1 data [38] was retrieved from GEO (GSE92742) and imported into R using the cmapR (v1.0.1) package (https://github.com/cmap/cmapR). Only the landmark genes were used for downstream analyses, because the imputed expressions of non-landmark genes showed discernible differences in distributions compared to the measured expressions of landmark genes. The expression differences between resistant and parental clones (query profiles) and expression differences across landmark genes in CMap between compound and vehicle (perturbation profiles) were compared using the cosine similarity measure (uncentered Pearson correlation). The null distribution of this similarity score was estimated by re-sampling genes in the query profiles with replacement. Additionally, we also compare the similarity scores between the query and a compound perturbation profile against the similarity scores between the query and all other compound perturbation profiles as follows. In CMap, each compound has several perturbation profiles generated in different cell lines, treatment dose, and duration. The perturbation profiles generated for the same compound are expected to be correlated. Therefore, the similarity score comparisons were performed using the correlation-adjusted t-test as implemented in limma [28]. The source code used for preprocessing the CMap data is available in a repository (https://github.com/djhshih/analysis-cmap), and the source code for the downstream analysis is available in another repository (https://github.com/djhshih/analysis-parpir-sum149-rna-seq).

Amplicon sequencing

DNA was extracted with NucleoSpin DNA RapidLyse (Macherey-Nagel, 740100), and the target region of *BRCA1* was amplified using PCR primers 5'-ACAGCGATACTTTCCCAGAGCT-3' and 5'-TGGGGTTTTCAAATGCTGCACA-3' with Amplicon-EZ adapters added. The PCR product was purified with NucleoSpin PCR Clean-up (Macherey-Nagel, 740609) and submitted for amplicon sequencing at Genewiz. Read pairs were aligned using bwa [39] mem (v0.7.17) to wildtype, mutant, or revertant allele within the amplified region of *BRCA1*. The numbers of R1 reads mapping uniquely to each allele with a quality score ≥5 were counted in each sample. The first sequencing batch showed an index cross-contamination rate of 0.40%, so the parental cells were re-cultured in isolation, and their DNA was re-extracted, PCR amplified, and submitted for sequencing in isolation, so as to eliminate the possibility of cross-contamination. Read depths of the revertant allele were higher due to the shorter amplicon, and this bias was corrected using total read depths across samples. The analysis source code is available in a repository (https://github.com/djhshih/analysis-parpir-sum149-amp-seq).

Immunofluorescence

Cells were seeded on glass cover slips and incubated in growth medium for 2-3 days. At harvest, the cells were fixed in 10% formalin for 10 min, permeabilized with 1% Triton X100 in PBS for 10 min, and blocked with 5% horse serum in PBS-T (0.05% Triton X100 in PBS) for 1 h. Following PBS washes, the slides were incubated with primary antibodies against vimentin (Abcam, ab92547, 1:250) or E-cadherin (CST, #3195, 1:200) at 4°C overnight. After PBS-T washes, the slides were incubated for 1 h with Alexa Fluor 568 secondary antibody (Thermo Fisher, A10042, 1:500), along with Alexa Fluor 488 Phalloidin (Thermo Fisher, A12379, 1:200). The slides were washed with PBS-T, stained with Hoechst (Invitrogen, H3570, 1:1000) for 10 min, and washed again before mounting on glass slides with Vecta-Shield medium (Vector Laboratories, H-1000) and subsequent fluorescence microscopy.

Drug sensitivity assay

Cells were seeded in 96-well plates at a density of 1000 cells per well in 3-4 replicates, allowed to adhere overnight, and treated with drugs, vehicle control, or no treatment for 6 days. Compounds were dissolved in DMSO, unless indicated otherwise. Cisplatin was dissolved in saline. During the incubation period, the outermost wells were filled with PBS. Subsequently, cell viability was assessed by PrestoBlue (Thermo Fisher, A13262). The cells were incubated at 37°C with PrestoBlue for up to 4 hours, and fluorescent signals were measured every hour by a microplate reader. The longest measurement time point before signal saturation was selected for analysis. Potentially contaminated wells were identified by outlier colour change, confirmed visually under an optical microscope, and flagged for exclusion.

Data normalization was performed independently for each plate, which contained blank, vehicle, and mock controls. After subtracting mean signal from blank wells, relative viability values were calculated by dividing treatments by vehicle controls. After normalization, the drc [40] package (v3.0) was used to fit four-parameter log-logistic functions to the data, estimate confidence bands, and determine IC50 (absolute ED50) values. The analysis source code is available in a repository (https://github.com/djhshih/cell-viability-tecan).

RAD51 foci formation assay

Cells were plated onto 4-well chamber slides and incubated overnight, followed by 50 nM talazoparib treatment. After 24 h of treatment, cells were fixed with 4% paraformaldehyde, and immunofluorescence was performed with primary antibodies against RAD51 (Abcam, ab63801, 1:1000) and gamma-H2AX (Sigma-Aldrich, #05-636, 1:1000) at 4°C overnight. Goat anti-rabbit TexasRed and goat anti-mouse FITC were used as secondary antibodies. DNA was counterstained by DAPI-containing mounting media (Vector Laboratories, H-2000). Fluorescence imaging was done using a Zeiss 710 confocal microscope.

Western blotting

Total protein was extracted with a urea lysis buffer (1 M Tris-HCl, pH 7.5, 8 M urea, 150 mM β-mercaptoethanol, and fresh protease inhibitors) and sonication. Following SDS-PAGE, western blotting was performed with primary antibodies against phospho-ERK (CST, #9101) or total ERK (CST, #4695), and secondary anti-rabbit antibody (Bio-Rad, #1706515).

Quantitative RT-PCR

The primers were selected from the PrimerBank [41] or designed with Primer3 [42], and they were ordered from Sigma-Aldrich (Table S3). The specificities of primer pairs were checked using Primer-BLAST [43]. Total RNA was extracted using the E.Z.N.A. Total RNA Kit I (Omega Bio-tek, #101319-242), and cDNA was synthesized with the iScript cDNA Synthesis Kit (Bio-Rad, #1708891). qPCR assays were performed with the amfiSure qGreen Q-PCR Master Mix (GenDEPOT, #Q5600-005), and relative expressions were estimated using the delta-delta Ct method with 18S rRNA as the internal control and the parental clone as the reference.

siRNA knockdown

MISSION predesigned siRNAs against target genes were purchased from Sigma-Aldrich. After seeding and overnight incubation, the cells were transfected with siRNAs using Lipofectamine (Thermo Fisher, #L3000008) and re-plated after 24 h for drug sensitivity assays with 4-5 days of drug, vehicle, or no treatment.

Revertant probability

We calculate the probability that a revertant cell emerges from a population of cancer cells by using the frequency of insertions in *BRCA1-/-* mutants reported previously [44]. We only consider the case in which the original loss-of-function is caused by a 1 bp deletion (as was observed in SUM149). Define g as the size of the sequencible genome, and r as the rescuable region of the gene (i.e. the revertant insertion must land in front the premature stop codon caused by the original frameshift mutation, and it must also not introduce a premature stop codon in front of the original mutation). Since r is an unknown parameter, we conservatively assume that it would be about 120 bp (with a range of 60-600 bp), which is equivalent to 20 codons (with a range of 10 to 100 codons) before and after the original

frameshift. Then, the probability that 1 of d insertions lands at the correct location is p_1 = Binomial (1; d, r/g). It is theoretically possible for m+3 insertions of 1 bp for some natural number m>0 to also restore the reading frame, but these probabilities only combine additively with p_1 and are negligible compared to p_1, so we do not consider them. Similarly, it is also possible for insertions of m+3 bps to rescue the 1 bp deletion, but the frequencies of these events are much lower than 1 bp insertions [44], so their contributions are much smaller. Because these additional scenarios are omitted, our revertant probability would be somewhat conservative. Given p_1, the probability that at least one revertant cell emerges from a population of n cancer cells after one generation is simply $p_r = 1-(1-p_1)^n$.

Statistical analysis

All statistical analyses were performed in the R environment (v3.6.3). Adjustments for multiple hypothesis testing were performed using the Benjamini-Hochberg method [45]. All other analyses have been described above in the relevant subsections.

Results

We derived and characterized the transcriptomes of resistant clones from the SUM149 cell line, which is a *BRCA1* homozygous mutant, triple-negative inflammatory breast cancer cell line (**Figure 1A**). The derived clones became stably resistant to talazoparib and other PARPi, even after extended maintenance in standard growth medium without PARPi (**Figures 1B**, S1). We characterized the parental and resistant clones by RNA sequencing, and gene set variation analysis revealed that the resistant clones acquired substantial heterogeneous transcriptomic changes across hallmark cancer pathways, while changes due to short-term talazoparib treatment were much more modest (**Figure 1C**). G2M checkpoint, E2F targets, and oxidative phosphorylation were strongly upregulated in a subset of resistant clones compared to the parental clone; however, they were not consistently significantly upregulated across all resistant clones (**Figures 1D**, **1E** and S2). Conversely, many pathways were downregulated in the resistant clones, including NFκB signaling, TGFβ signaling, KRAS signaling, and epithelial mesenchymal transition (EMT) (**Figures 1D**, S2).

We next examined the expression levels of specific genes that are important in PARPi resistance. Since inactivation of the 53BP1-RIF1-REV7 axis has been shown to contribute to PARPi resistance [46], we specifically compared the expressions of these genes in the resistant clones against the parental clone. REV7 (MAD2L2) was downregulated in most resistant clones, while BRCA1 transcript level was also restored in most resistant clones (Figures S3, S4). These results show that the PARPi-resistant clones suppressed the 53BP1-RIF1-REV7 axis, restored *BRCA1* expression, or both. Additionally, cyclin-dependent kinases (CDKs) play an important role in DNA damage repair [47], so we tested the differential expressions of CDKs in the resistant clones vs. the parental (Figure S4). CDK3, CDK5, CDK8, CDK9, CDK12, CDK20 were modestly upregulated in some resistant clones, CDK18 was downregulated, and other CDKs did not exhibit a consistent pattern of change across the resistant clones.

While DNA repair and other pathways showed inconsistent transcriptional changes across the resistant clones, KRAS and EMT pathways showed consistent downregulation in all resistant clones (**Figure 1E**). Heterogeneous levels of phospho-ERK were detected across the resistant clones by Western blotting (Figure S5). Furthermore, as EMT is widely known to be associated with drug resistance, its downregulation in the PARPi-resistant clones was quite surprising. We therefore assessed protein markers of mesenchymal and epithelial phenotypes by immunofluorescence. The parental clone contained a high proportion of vimentin$^+$ (mesenchymal) cells, while resistant clones showed considerably fewer vimentin$^+$ cells (**Figures 1F**, S6). Additionally, cell surface expression of E-cadherin remained low in parental and resistant clones (Figure S6). Taken together, these results suggest that the PARPi-resistant clones have partially reversed epithelial-to-mesenchymal transition and lost mesenchymal characteristics.

Next, we sought to identify drugs that may be used in combination with PARPi in order to overcome drug resistance. We hypothesized that transcriptional changes acquired by the

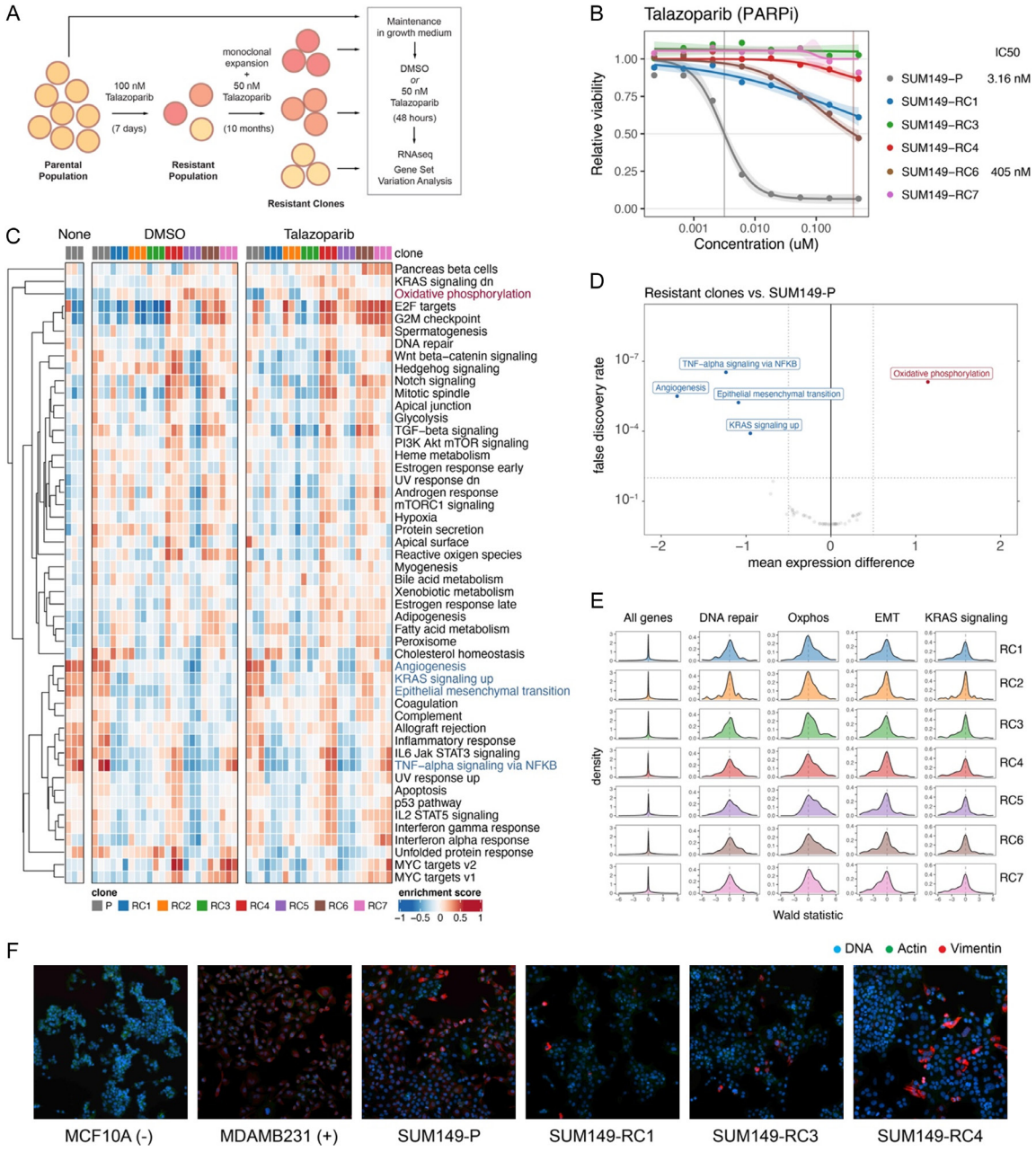

Figure 1. PARPi-resistant cancer clones undergo partial mesenchymal to epithelial transition. A. Workflow for deriving PARPi resistant clones and generating RNA-seq data. B. Sensitivities of parental and PARPi-resistant clones to talazoparib, relative to DMSO vehicle control. Sensitivities to other PARPi are provided in Figure S1. C. Gene set variational analysis reveals relative enrichment and depletion of hallmark biological processes. Heatmap colours reflect relative enrichment scores across samples. After stable PARPi-resistant clones had been derived, the resistant and parental clones were treated with DMSO or talazoparib for 48 h, followed by total RNA harvest and RNA-seq analysis. D. Volcano plots of enriched and depleted pathways by competitive analyses comparing differential gene expression statistics inside vs. outside each gene set using CAMERA. Expression differences are between all resistant clones and the parental. Results for each resistant clone vs. the parental are shown in Figure S2. E. Density plots of differential gene expression Wald statistics of each resistant clone vs. parental within indicated gene sets, as estimated by DESeq2. F. Immunofluorescence of MCF10A (epithelial) and MDAMB231 (mesenchymal) cells, parental SUM149 cells, and PARPi-resistant cells, staining for DNA (Hoechst), actin (phalloidin), and vimentin. RC, PARPi-resistant clone. P, parental clone.

resistant clones allowed them to become resistant to PARP inhibitors, and reversing these transcriptional changes could overcome resistance (**Figure 2A**). Therefore, we used the

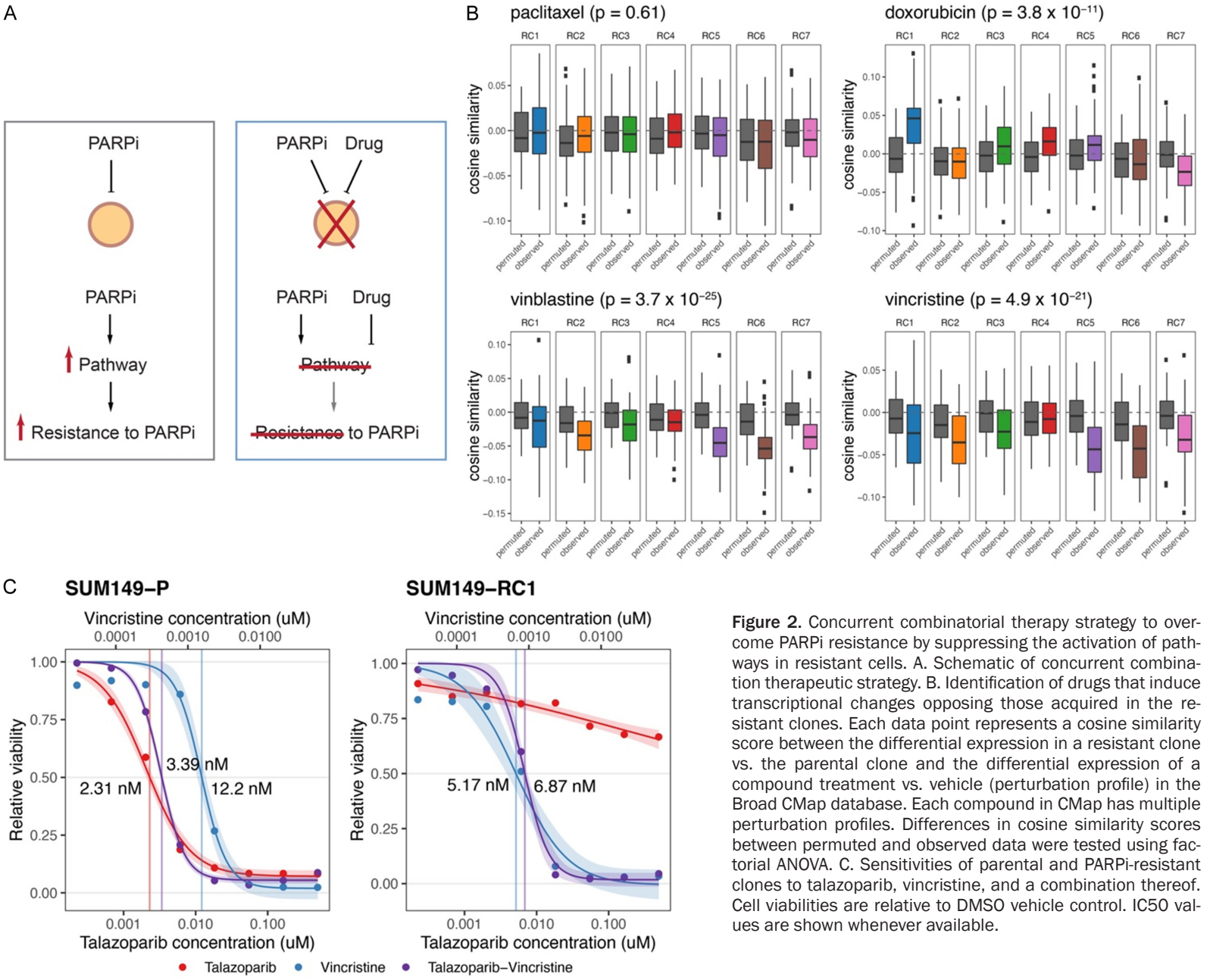

Figure 2. Concurrent combinatorial therapy strategy to overcome PARPi resistance by suppressing the activation of pathways in resistant cells. A. Schematic of concurrent combination therapeutic strategy. B. Identification of drugs that induce transcriptional changes opposing those acquired in the resistant clones. Each data point represents a cosine similarity score between the differential expression in a resistant clone vs. the parental clone and the differential expression of a compound treatment vs. vehicle (perturbation profile) in the Broad CMap database. Each compound in CMap has multiple perturbation profiles. Differences in cosine similarity scores between permuted and observed data were tested using factorial ANOVA. C. Sensitivities of parental and PARPi-resistant clones to talazoparib, vincristine, and a combination thereof. Cell viabilities are relative to DMSO vehicle control. IC50 values are shown whenever available.

Broad Connectivity Map (CMap) database of compound perturbation profiles to look for drugs that perturb transcriptional programs (as compared to vehicle control) in a direction that is opposite to the transcriptional changes observed in the resistant clones (as compared to the parental). For these comparisons, we chose the cosine similarity measure (uncentered Pearson correlation), because the feature of primary interest is the direction of the transcriptional differences, rather than the magnitude. Indeed, the magnitude of transcriptional differences could be strongly affected by platform differences in signal gain and saturation characteristics. Accordingly, we looked for drugs whose CMap perturbation profiles are anti-correlated with transcriptional differences observed in resistant clones. Among drugs known to be effective in breast cancer, paclitaxel showed no similarity with the transcriptional difference profile of the resistance clone, and doxorubicin showed a heterogeneous pattern of correlations across the clones, whereas vinblastine and vincristine showed a strong and consistent anti-correlation (**Figure 2B**; Table S1). We thus tested by cell viability assays whether vincristine would be effective in concurrent combination with talazoparib. However, vincristine did not synergize with talazoparib treatment in either the parental or resistance clone (**Figure 2C**). Furthermore, we also investigated whether knockdown of specific genes that are highly upregulated in the PARPi-resistant clones can sensitize the resistant clones to PARP inhibitors. However, the siRNA knockdown of several of such genes, including *BAX*, *CALML5*, *ERRFI1*, *ESRP1*, *TSC22D3*, and *YWHAQ*, did not affect the sensitivities of resistant cells to PARP inhibitors, as compared to siRNA control (Figure S7). Despite these endeavors, we did not identify promising leads for concurrent combinatorial therapy to overcome PARPi resistance.

Given our unsuccessful attempts at identifying an effective concurrent combinatorial therapy, we hoped to better understand the mechanism of resistance to PARPi. Inspection of RNA-seq reads at the *BRCA1* exon 10 locus confirmed the known [48] homozygous 1-bp frameshift deletion in the parental clone causing a premature stop codon (p.P724fs*12) and nonsense mediated decay (**Figure 3A**). The resistant clones not only inherited the same frameshift deletion but also showed a second deletion of 36 bp and a 1 bp insertion (**Figures 3A**, S8). This secondary compound indel restored the reading frame of the *BRCA1* gene, which allowed *BRCA1* transcript levels to be restored in the resistant clones (Figure S4). The revertant DNA allele was confirmed by amplicon sequencing (**Figure 3B**). The parental clone had bi-allelic inactivation of *BRCA1* due to p.P724fs*12, while the resistant clones harboured the same revertant allele of *BRCA1* (**Figure 3B**). Allele frequencies of the revertant mutation were 50% in the resistant clones, which suggests that the revertant mutation is heterozygous clonal (**Figure 3B**). Ultra deep sequencing revealed that parental clone contained a subclone harbouring the revertant allele at a cancer cell fraction of 2.43×10^{-5}, or 1 in 40,000 cells (**Figure 3C**). To assess the activity of revertant BRCA1 protein in the resistant clones, we assessed γ-H2AX and RAD51 foci formation following 24 h of talazoparib treatment. As expected, the resistant clones exhibited greater numbers of RAD51 foci and higher fractions of RAD51 positive nuclei, indicating higher homologous repair activities, compared to the parental clone (Figure S9). Further, the resistant clones have fewer γ-H2AX foci and lower fractions of γ-H2AX positive nuclei, indicating fewer unrepaired double-strand breaks, compared to the parental clone (Figure S9). Importantly, the fractions of γ-H2AX positive and RAD51 negative nuclei in the resistant clones were lower than those in the parental clone and have been nearly restored to levels observed in the BRCA wild-type cell line MCF10A (**Figure 3D**). Accordingly, based on the mechanism of action of PARPi [11], this restoration of homologous repair in *BRCA1* revertant cells would eliminate their sensitivity to PARPi treatment (**Figure 3E**). Furthermore, we characterized how EMT and KRAS signaling activities changed in response to short-term and long-term PARPi treatment. In the parental and resistant clones, short-term (48 hours) talazoparib treatment increased EMT and KRAS signaling, while the extended (10 months) talazoparib treatment that the resistant clones experienced has caused a transcriptional reversal and dramatic downregulation in EMT and KRAS signaling compared to the parental clone (**Figure 3F**). Interestingly, the short-term response to talazoparib in terms of the upregulation of EMT and KRAS signaling

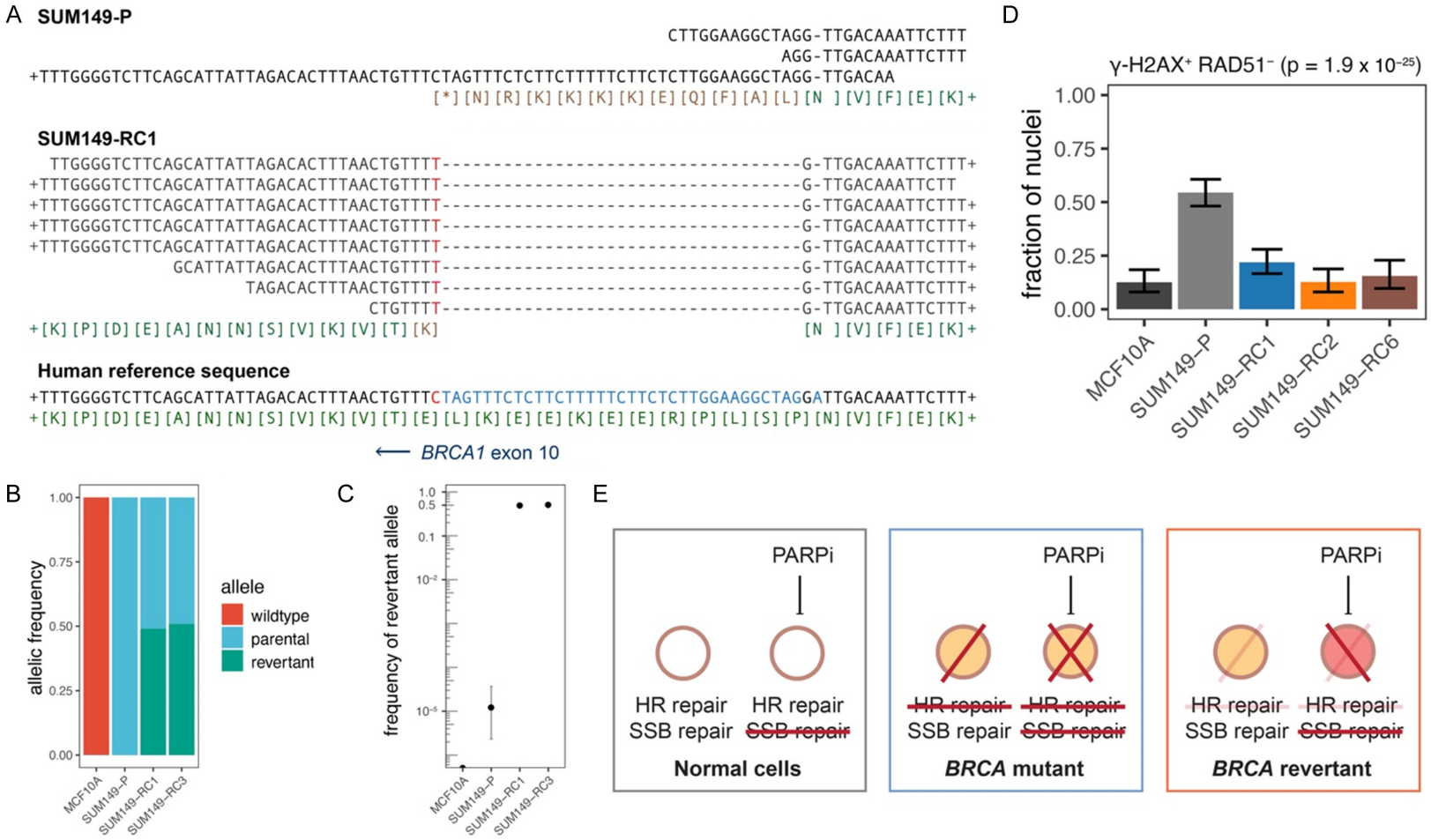
A
SUM149-P
CTTGGAAGGCTAGG-TTGACAAATTCTTT
AGG-TTGACAAATTCTTT
+TTTGGGGTCTTCAGCATTATTAGACACTTTAACTGTTTCTAGTTTCTCTTCTTTTTCTTCTCTTGGAAGGCTAGG-TTGACAA
[*][N][R][K][K][K][K][E][Q][F][A][L][N][V][F][E][K]+
SUM149-RC1
TTGGGGTCTTCAGCATTATTAGACACTTTAACTGTTTT----------G-TTGACAAATTCTTT+
+TTTGGGGTCTTCAGCATTATTAGACACTTTAACTGTTTT----------G-TTGACAAATTCTT
+TTTGGGGTCTTCAGCATTATTAGACACTTTAACTGTTTT----------G-TTGACAAATTCTTT+
+TTTGGGGTCTTCAGCATTATTAGACACTTTAACTGTTTT----------G-TTGACAAATTCTTT+
+TTTGGGGTCTTCAGCATTATTAGACACTTTAACTGTTTT----------G-TTGACAAATTCTTT+
GCATTATTAGACACTTTAACTGTTTT----------G-TTGACAAATTCTTT+
TAGACACTTTAACTGTTTT----------G-TTGACAAATTCTTT+
CTGTTTT----------G-TTGACAAATTCTTT+
+[K][P][D][E][A][N][N][S][V][K][V][T][K]
[N][V][F][E][K]+
Human reference sequence
+TTTGGGGTCTTCAGCATTATTAGACACTTTAACTGTTTCTAGTTTCTCTTCTTTTTCTTCTCTTGGAAGGCTAGGATTGACAAATTCTTT+
+[K][P][D][E][A][N][N][S][V][K][V][T][E][L][K][E][E][K][E][E][R][P][L][S][P][N][V][F][E][K]+
BRCA1 exon 10
D
γ-H2AX+ RAD51− (p = 1.9 x 10−25)
fraction of nuclei
1.00
0.75
0.50
0.25
0.00
MCF10A
SUM149–P
SUM149–RC1
SUM149–RC2
SUM149–RC6
B
allelic frequency
1.00
0.75
0.50
0.25
0.00
allele
wildtype
parental
revertant
MCF10A
SUM149–P
SUM149–RC1
SUM149–RC3
C
frequency of revertant allele
1.0
0.5
0.1
10−2
10−5
MCF10A
SUM149–P
SUM149–RC1
SUM149–RC3
E
PARPi
HR repair
SSB repair
SSB repair
Normal cells
PARPi
HR repair
SSB repair
SSB repair
BRCA mutant
PARPi
HR repair
SSB repair
SSB repair
BRCA revertant

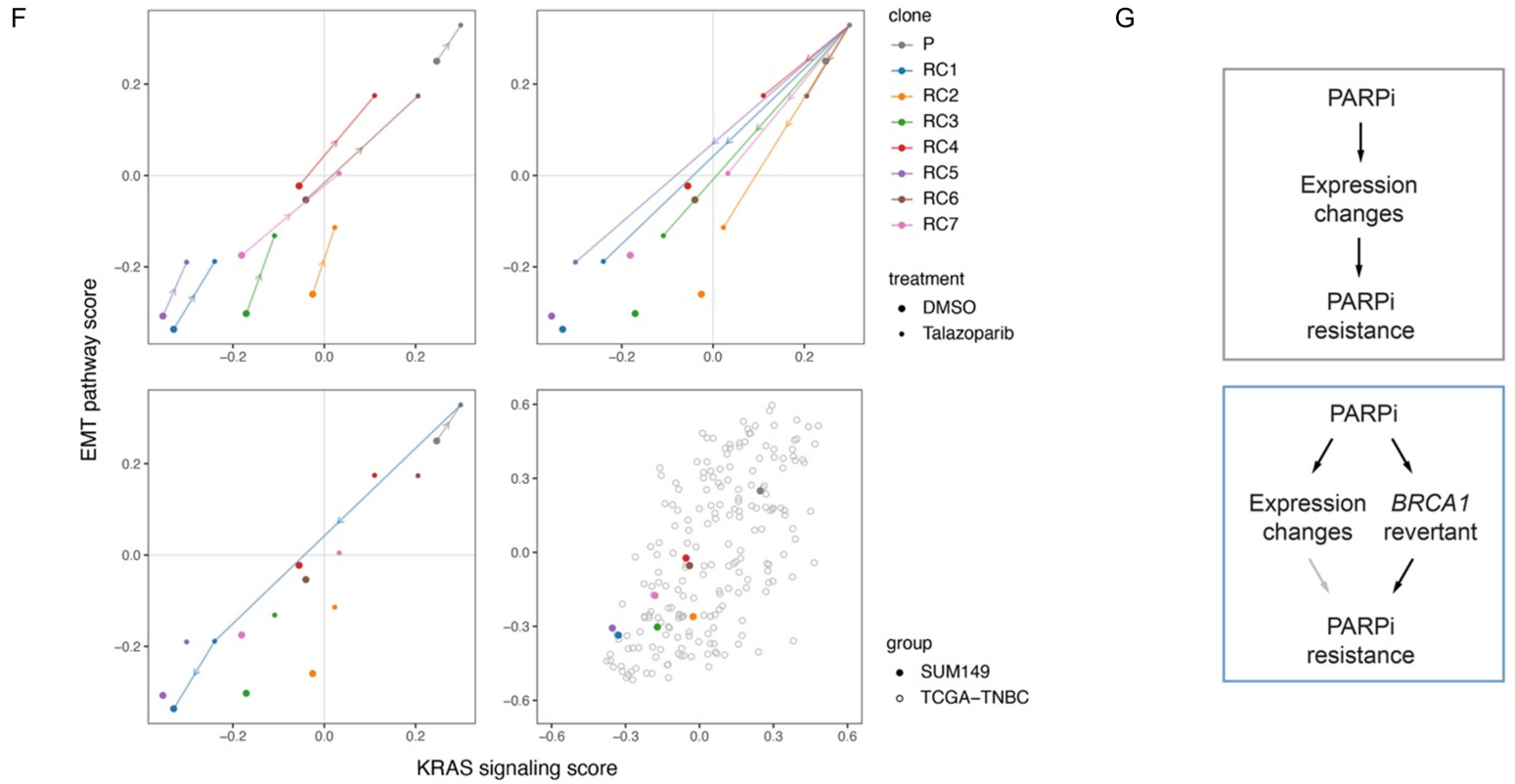

Figure 3. PARPi-resistant cancer clones derive from pre-existing *BRCA1* revertant and reverse transcriptional response to PARPi. A. RNA-seq reads from parental and resistant clone mapping to the *BRCA1* exon 10 locus harbouring the frameshift deletion. Bottom row of each block shows the translated amino acid sequence. The revertant reads seen in RC1 are observed in all resistant clones (Figure S8). B. Frequency of wildtype, parental, and revertant alleles determined by amplicon sequencing at 40,000 to 100,000 read depth. C. Frequency of the revertant allele on log scale. Bars represent 95% Clopper-Pearson confidence intervals. D. Restoration of double-strand break by homologous repair in PARPi-resistant clones. Bars represent proportions of nuclei with ≥10 γ-H2AX foci and <10 RAD51 foci. Resistant clones have significant lower fractions of γ-H2AX^{+} RAD51^{-} nuclei vs. parental (Fisher's exact test). Representative immunofluorescence images and additional quantification results are shown in Figure S9. E. Mechanism of PARPi resistance in the *BRCA1* revertant. F. Scatter plots of enrichment scores for the epithelial to mesenchymal (EMT) pathway and the KRAS signaling pathway. Arrows represent directions of change from vehicle to talazoparib treatment (*top left*), from parental to resistant clones under talazoparib treatment (*top right*), and from parental to RC1 during the derivation of resistant clones (*bottom left*). Enrichment scores of triple-negative breast cancer samples from the TCGA (*bottom right*). G. Competing mechanisms for PARPi resistance.

remains intact in the resistant clones (**Figure 3F**). While the parental clone had EMT and KRAS signaling activities in the upper quartile compared to triple-negative breast cancers in the TCGA, the resistant clones had among the lowest EMT and KRAS signaling activities (**Figure 3F**). Collectively, these results suggest that the expression changes observed in the resistant clones may not actually be major drivers of PARPi resistance, given that the *BRCA1* revertant mutation would be sufficient to explain PARPi resistance (**Figure 3G**).

In light of the revelation that the transcriptional changes observed in the resistant clones likely did not confer PARPi resistance, we revised our strategy for overcoming PARPi resistance to a sequential therapeutic strategy that exploits the vulnerability induced by transcriptional adaptation to prior treatments (**Figure 4A**). Under this model, we hypothesize that transcriptional adaptation may lead to an exploitable deficiency in a particular pathway. Accordingly, we look for drugs that perturb transcriptional profiles in the same direction as the transcriptional changes acquired in the resistance clone, and we quantify this correlation by the cosine similarity measure. In other words, we seek to identify a compound that reinforces the deficiencies induced by prior treatment. Screening across the compounds in the CMap database, we identified many compounds that target the Ras-Raf-MEK-ERK pathway among the top hits (**Figure 4B**; Table S2). The perturbation profiles of the MEK inhibitor selumetinib were correlated with transcriptional changes across all resistant clones (**Figure 4C**). Importantly, PARPi-resistant clones were significantly more sensitive to selumetinib compared to the parental clone, which suggests that selumetinib would be a promising lead for overcoming PARPi resistance in sequential combinatorial therapy (**Figure 4D**). As expected, concurrent combinatorial therapy (which is not consistent with the proposed sequential reinforcement strategy) with talazoparib and selumetinib did not result in synergy (Figure S10).

Discussion

The propensity of PARPi to specifically kill *BRCA1/2* mutant cells is perhaps also the biggest weakness of PARPi. This class of drugs target cancer cells defective in homologous repair due to the loss of *BRCA1/2* function, which may be restored by revertant mutations in *BRCA1/2*. Such revertant mutations are not infrequently observed in breast and ovarian cancers [49-53]. Here, we showed that a *BRCA1* heterozygous revertant subclone may be present at an extremely low cancer cell fraction of 1 in 40,000 that would require a sequencing depth of 100,000× in order to detect reliably. This sequencing depth is multiple orders of magnitude higher than the average depths typically achieved in targeted clinical sequencing [54-56] which would make the detection of *BRCA1/2* revertant very challenging prior to treatment.

After a *BRCA1/2* revertant clone emerges in germline *BRCA1/2* mutant patients, the therapeutic window for PARPi would disappear because *BRCA1/2* revertants would have the same number of functional copies of *BRCA1/2* as normal cells. That is, the revertant cancer cells and the normal cells would both have one functional copy of *BRCA1/2*. Ideally, one would like to find a drug that can reverse the PARPi resistance phenotype; however, due to the equivalence in *BRCA1/2* gene dosage, attempts to reverse *BRCA1/2* function in the cancer cells would likely also cause cytotoxic effects on normal cells. Accordingly, it may be very difficult to find drugs that can be administered concurrently in combination with PARPi to kill the tumour cells while sparing the normal cells.

One strategy to circumvent PARPi resistance might be to use a combinatorial treatment up front so as to prevent the emergence of *BRCA1/2* revertants. However, as we have shown, the *BRCA1/2* revertants were present at extremely low frequency before drug treatment, consistent with prior reports [51]. A likely explanation for this is that biallelic *BRCA1/2* mutants are defective in homologous repair such that the mutant cells can now only repair double-strand breaks via the error-prone non-homologous end-joining pathway, which often introduces DNA indels. Consequently, the chance that at least one cell within a residual tumour mass would have a frameshift-restoring frameshift in *BRCA1/2* is non-negligible. Based on the frequency of insertions previously reported in *BRCA1* mutants [44], we estimate that the probability that a revertant mutation would restore a 1 bp deletion in *BRCA1* in at least one cell out of a million cells

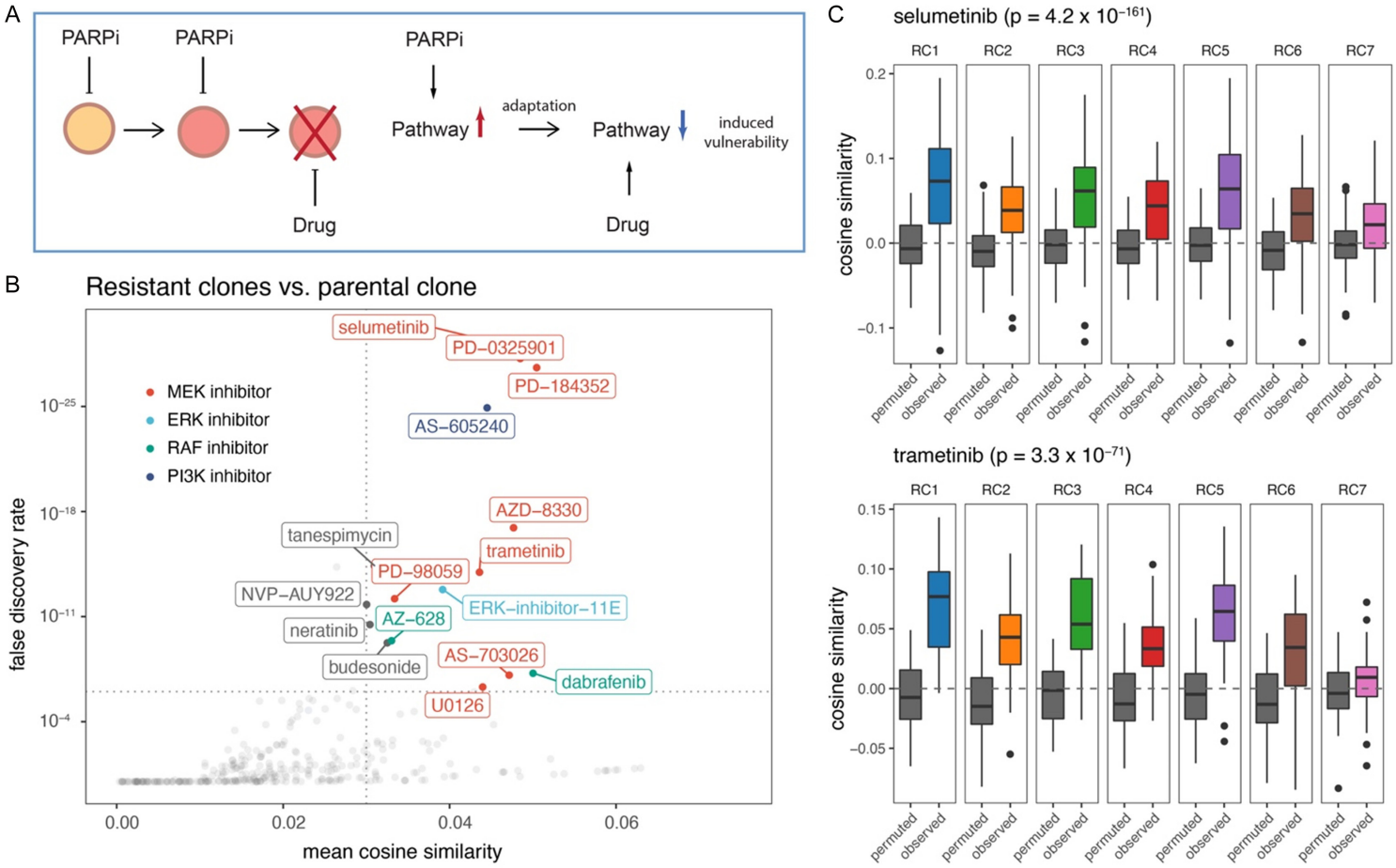

Figure 4. Therapeutic strategy that exploits vulnerability induced by prior PARPi treatment. A. Schematic of sequential combination therapeutic strategy. B. Identification of drugs that reinforce transcriptional adaptation to PARPi treatment by comparison to perturbation profiles in Broad CMap. Statistical significance was tested by comparing cosine similarities between differential expressions in resistant clones vs. parental and perturbation profiles involving each compound vs. cosine similarities involving other all compounds using the correlation-adjusted t-test. Dotted lines represent mean cosine similarity threshold (vertical) and false discovery rate at 10^{-6} (horizontal). C. Box plots of cosine similarity scores between differential expressions in resistant clones vs. parental and differential expressions of drug treatment vs. vehicle in Broad CMap. Differences in cosine similarity scores between permuted and observed data were tested using factorial ANOVA. D. Sensitivities of parental and PARPi-resistant clones to selumetinib. Cell viabilities are relative to DMSO vehicle control. IC50 values are shown whenever available.

is about 18% after one generation (Figure S11). Detecting this rare (heterozygous) revertant mutation with at least two sequencing reads would require a minimum sequencing depth of 5,000,000× in a tumour with ≤20% normal contamination. Therefore, it may be technically infeasible to prevent the emergence of *BRCA1/2* revertant cancer cells.

We show here that multiple PARPi-resistant clones from an inflammatory triple-negative breast cancer cell line have transcriptional adaptations in EMT and Ras signaling. Initially after short-term talazoparib treatment, EMT was transiently upregulated in the parental clone; however, long-term treatment eventually caused EMT to be reversed in cancer cells that gave rise to the resistant clones. Since EMT has been strongly associated with drug resistance [57], this reversal of EMT is highly unlikely to have contributed to PARPi resistance, especially in light of the emergence of the *BRCA1* revertant mutation. Similarly, Ras signaling is essential for cell growth and proliferation, and its downregulation has not been linked to PARPi resistance. Nonetheless, this transcriptional adaptation causes a deficiency in Ras signaling. Consistent with this notion, the PARPi-resistant clones had among the lowest transcriptional scores of KRAS signaling compared to triple-negative breast cancers in the TCGA, whereas the parental clone had among the highest scores. In turn, this induced deficiency renders the cancer cells vulnerable to further inhibition of components in this pathway, namely ERK and MEK. By reinforcing this induced deficiency in Ras signaling, MEK inhibitors can now effectively suppress these cancer cells. Hence, reinforcing the induced deficiency in Ras signaling represents a promising alternative strategy to overcome acquired resistance after long-term PARPi treatment.

Interestingly, our results indicate that KRAS signaling score can change dynamically in response to PARPi treatment, even in opposite directions depending on the duration of treatment. This dynamic response in KRAS signaling was surprising, because PARPi targets DNA damage repair and does not directly target the Ras pathway. Accordingly, KRAS signaling would be a key pathway to monitor throughout PARPi treatment, because high KRAS signaling score is associated with better patient survival in triple-negative breast cancer [58].

Our results also indicate that EMT status can change dynamically in response to PARPi treatment. We showed that short-term (48 h) PARPi treatment initially causes the SUM149 cells to undergo EMT, similar to previous findings by Han *et al*. [17]. The authors found that 72 h of olaparib treatment caused several breast cancer cell lines to undergo EMT, and they showed similar results for rucaparib and talazoparib [17]. Importantly, we showed here that long-term (several months) PARPi treatment causes the partial reversal of EMT in SUM149 across several clones. This result, while surprising, is not entirely unprecedented, as olaparib has been shown to revert TGF-β induced EMT in mouse mammary cells [59].

Given that PARPi are used for maintenance therapy over long periods of time, it would be clinically important to track over time its effects on key pathways, such as Ras and EMT signaling, particularly since the direction of transcriptional and signaling changes may reverse. These dynamic transcriptional changes may vary across patients and would have important implications for therapeutic decision-making. Transcriptomics would offer an effective approach to monitor key changes in molecular pathways and pathobiological processes during cancer treatment [60-64].

We caution that some of our biological findings may have limited applicability to breast cancer in general, given that we focused on BRCA mutant triple-negative inflammatory breast cancer, which represents only about 0.3% of breast cancer patients [65]. Nonetheless, this is a very aggressive form of breast cancer that has few treatment options beside PARPi. It is therefore all the more important to find an effective strategy to overcome PARPi resistance for these patients, while taking clonal heterogeneity into account so that we may minimize the chance of additional resistance. While we show that PARPi resistant clones of SUM149 develop selumetinib sensitivity, breast tumors from other patients may develop different sensitivities, given that breast cancers show substantial variability among patients. We would thus advocate that the transcriptomics of resistant tumors be characterized for each patient. Indeed, our bioinformatic strategy may serve as a motivating example towards precision oncology.

To emphasize, we anticipate that our strategy of exploiting secondary vulnerabilities by pharmacological reinforcement of transcriptional adaptation can be applied to other targeted therapies. A critical weakness of targeted therapy is that cancers often eventually develop resistance. When the resistant clone develops a mutation that directly nullifies the anti-cancer agent (such as a *BRCA1/2* revertant mutation and PARPi), options to overcome therapeutic resistance would be limited. However, as we have shown with PARPi, the anti-cancer agent may cause the cancer cells to undergo transcriptional adaptation that exposes a deficiency or vulnerability. In support of the broader applicability of the pharmacological reinforcement strategy, Ibrahim *et al.* have shown that PI3K inhibition impairs the expression of *BRCA1/2* in breast cancer, thus inducing a sensitivity to PARP inhibition (which targets *BRCA1/2*) [66]. Our bioinformatic approach of comprehensive transcriptomic characterization of drug resistant clones and systematic comparison with compound perturbation profiles would vastly accelerate the discovery process. The generalization of our bioinformatic approach to acquired resistance against other anti-cancer drugs may require the incorporation of additional compound screening criteria, some of which may be context-specific. It would also be informative to investigate the sufficient conditions under which the pharmacological reinforcement of transcriptional adaptations would yield a promising lead for sequential treatment regimes. In the future, this paradigm for discovering new combinatorial therapeutic strategies would greatly improve the treatment of tumours with acquired drug resistance.

Acknowledgements

D.J.H.S. has been supported by a fellowship from the Gulf Coast Consortia, on the Computational Cancer Biology Training Program (CPRIT Grant No. RP170593). D.J.M. was supported by Susan G. Komen PDF17483544. S.Y.L. has been supported by an award from the George and Barbara Bush Endowment for Innovative Cancer Research. This research was supported in part by the National Cancer Institute grant 5R01CA211615 (L.Y.), the Cancer Prevention and Research Institute of Texas grant RP170668 (W.J.Z.), the National Center for Advancing Translational Sciences grant NIH/NCATS 1 UL1 TR003167 01 (W.J.Z.), and the Ministry of Science and Technology grant MOST 110-2639-B-039-001-ASP (M.C.H.). K.A.D. was partially supported by NCI Grant P30 CA016672, as well as NIH grants UL1TR003167 and 5R01GM122775. The MD Anderson Sequencing and Microarray facility was supported by the core grant CA016672 (SMF). We thank Joseph Nasser (Broad Institute) for fruitful discussions.

Disclosure of conflict of interest

None.

Address correspondence to: Shiaw-Yih Lin, Department of Systems Biology, University of Texas MD Anderson Cancer Center, 6565 MD Anderson Blvd, Z10.3034, Houston, TX 77030-4009, USA. Tel: 713-563-4217; E-mail: sylin@mdanderson.org

References

[1] Wang L, Zhu X, Li L, Li L, Fu L, Li Y, Fu H, Chen X and Lou L. TSL-1502, a glucuronide prodrug of a poly (ADP-ribose) polymerase (PARP) inhibitor, exhibits potent anti-tumor activity in preclinical models. Am J Cancer Res 2021; 11: 1632-1645.

[2] Lemjabbar-Alaoui H, Peto CJ, Yang YW and Jablons DM. AMXI-5001, a novel dual parp1/2 and microtubule polymerization inhibitor for the treatment of human cancers. Am J Cancer Res 2020; 10: 2649-2676.

[3] Moore K, Colombo N, Scambia G, Kim BG, Oaknin A, Friedlander M, Lisyanskaya A, Floquet A, Leary A, Sonke GS, Gourley C, Banerjee S, Oza A, González-Martín A, Aghajanian C, Bradley W, Mathews C, Liu J, Lowe ES, Bloomfield R and DiSilvestro P. Maintenance olaparib in patients with newly diagnosed advanced ovarian cancer. N Engl J Med 2018; 379: 2495-2505.

[4] Golan T, Hammel P, Reni M, Van Cutsem E, Macarulla T, Hall MJ, Park JO, Hochhauser D, Arnold D, Oh DY, Reinacher-Schick A, Tortora G, Algül H, O'Reilly EM, McGuinness D, Cui KY, Schlienger K, Locker GY and Kindler HL. Maintenance olaparib for germline-mutated metastatic pancreatic cancer. N Engl J Med 2019; 381: 317-327.

[5] Mateo J, Carreira S, Sandhu S, Miranda S, Mossop H, Perez-Lopez R, Nava Rodrigues D, Robinson D, Omlin A, Tunariu N, Boysen G, Porta N, Flohr P, Gillman A, Figueiredo I, Paulding C, Seed G, Jain S, Ralph C, Protheroe A, Hussain S, Jones R, Elliott T, McGovern U, Bianchini D, Goodall J, Zafeiriou Z, Williamson CT, Ferraldeschi R, Riisnaes R, Ebbs B, Fowler G, Roda D, Yuan W, Wu YM, Cao X, Brough R,

Pemberton H, A'Hern R, Swain A, Kunju LP, Eeles R, Attard G, Lord CJ, Ashworth A, Rubin MA, Knudsen KE, Feng FY, Chinnaiyan AM, Hall E and de Bono JS. DNA-repair defects and olaparib in metastatic prostate cancer. N Engl J Med 2015; 373: 1697-1708.

[6] Coleman RL, Oza AM, Lorusso D, Aghajanian C, Oaknin A, Dean A, Colombo N, Weberpals JI, Clamp A, Scambia G, Leary A, Holloway RW, Gancedo MA, Fong PC, Goh JC, O'Malley DM, Armstrong DK, Garcia-Donas J, Swisher EM, Floquet A, Konecny GE, McNeish IA, Scott CL, Cameron T, Maloney L, Isaacson J, Goble S, Grace C, Harding TC, Raponi M, Sun J, Lin KK, Giordano H and Ledermann JA; ARIEL3 investigators. Rucaparib maintenance treatment for recurrent ovarian carcinoma after response to platinum therapy (ARIEL3): a randomised, double-blind, placebo-controlled, phase 3 trial. Lancet 2017; 390: 1949-1961.

[7] Litton JK, Rugo HS, Ettl J, Hurvitz SA, Gonçalves A, Lee KH, Fehrenbacher L, Yerushalmi R, Mina LA, Martin M, Roché H, Im YH, Quek RGW, Markova D, Tudor IC, Hannah AL, Eiermann W and Blum JL. Talazoparib in patients with advanced breast cancer and a germline BRCA mutation. N Engl J Med 2018; 379: 753-763.

[8] Mirza MR, Monk BJ, Herrstedt J, Oza AM, Mahner S, Redondo A, Fabbro M, Ledermann JA, Lorusso D, Vergote I, Ben-Baruch NE, Marth C, Mądry R, Christensen RD, Berek JS, Dørum A, Tinker AV, du Bois A, González-Martín A, Follana P, Benigno B, Rosenberg P, Gilbert L, Rimel BJ, Buscema J, Balser JP, Agarwal S and Matulonis UA; ENGOT-OV16/NOVA Investigators. Niraparib maintenance therapy in platinum-sensitive, recurrent ovarian cancer. N Engl J Med 2016; 375: 2154-2164.

[9] Bryant HE, Schultz N, Thomas HD, Parker KM, Flower D, Lopez E, Kyle S, Meuth M, Curtin NJ and Helleday T. Specific killing of BRCA2-deficient tumours with inhibitors of poly(ADP-ribose) polymerase. Nature 2005; 434: 913-917.

[10] Michelena J, Lezaja A, Teloni F, Schmid T, Imhof R and Altmeyer M. Analysis of PARP inhibitor toxicity by multidimensional fluorescence microscopy reveals mechanisms of sensitivity and resistance. Nat Commun 2018; 9: 2678.

[11] Helleday T. The underlying mechanism for the PARP and BRCA synthetic lethality: clearing up the misunderstandings. Mol Oncol 2011; 5: 387-393.

[12] Yelamos J, Farres J, Llacuna L, Ampurdanes C and Martin-Caballero J. PARP-1 and PARP-2: New players in tumour development. Am J Cancer Res 2011; 1: 328-346.

[13] Sun C, Fang Y, Yin J, Chen J, Ju Z, Zhang D, Chen X, Vellano CP, Jeong KJ, Ng PK, Eterovic AKB, Bhola NH, Lu Y, Westin SN, Grandis JR, Lin SY, Scott KL, Peng G, Brugge J and Mills GB. Rational combination therapy with PARP and MEK inhibitors capitalizes on therapeutic liabilities in mutant cancers. Sci Transl Med 2017; 9: eaal5148.

[14] Fang Y, McGrail DJ, Sun C, Labrie M, Chen X, Zhang D, Ju Z, Vellano CP, Lu Y, Li Y, Jeong KJ, Ding Z, Liang J, Wang SW, Dai H, Lee S, Sahni N, Mercado-Uribe I, Kim TB, Chen K, Lin SY, Peng G, Westin SN, Liu J, O'Connor MJ, Yap TA and Mills GB. Sequential therapy with PARP and WEE1 inhibitors minimizes toxicity while maintaining efficacy. Cancer Cell 2019; 35: 851-867, e857.

[15] Li J, Zhi X, Chen S, Shen X, Chen C, Yuan L, Guo J, Meng D, Chen M and Yao L. CDK9 inhibitor CDKI-73 is synergetic lethal with PARP inhibitor olaparib in BRCA1 wide-type ovarian cancer. Am J Cancer Res 2020; 10: 1140-1155.

[16] Chu YY, Yam C, Chen MK, Chan LC, Xiao M, Wei YK, Yamaguchi H, Lee PC, Han Y, Nie L, Sun X, Moulder SL, Hess KR, Wang B, Hsu JL, Hortobagyi GN, Litton J, Chang JT and Hung MC. Blocking c-Met and EGFR reverses acquired resistance of PARP inhibitors in triple-negative breast cancer. Am J Cancer Res 2020; 10: 648-661.

[17] Han Y, Li CW, Hsu JM, Hsu JL, Chan LC, Tan X and He GJ. Metformin reverses PARP inhibitors-induced epithelial-mesenchymal transition and PD-L1 upregulation in triple-negative breast cancer. Am J Cancer Res 2019; 9: 800-815.

[18] Liang Y, Yu L, Zhang D, Zhao X, Gao H, Slagle BL, Goss JA, Wang X, Li K and Lin SY. BRIT1 dysfunction confers synergistic inhibition of hepatocellular carcinoma by targeting poly (ADP-ribose) polymerases and PI3K. Am J Cancer Res 2020; 10: 1900-1918.

[19] Yin Y, Shen Q, Zhang P, Tao R, Chang W, Li R, Xie G, Liu W, Zhang L, Kapoor P, Song S, Ajani J, Mills GB, Chen J, Tao K and Peng G. Chk1 inhibition potentiates the therapeutic efficacy of PARP inhibitor BMN673 in gastric cancer. Am J Cancer Res 2017; 7: 473-483.

[20] Shao B, Li CW, Lim SO, Sun L, Lai YJ, Hou J, Liu C, Chang CW, Qiu Y, Hsu JM, Chan LC, Zha Z, Li H and Hung MC. Deglycosylation of PD-L1 by 2-deoxyglucose reverses PARP inhibitor-induced immunosuppression in triple-negative breast cancer. Am J Cancer Res 2018; 8: 1837-1846.

[21] Suárez-Arroyo IJ, Feliz-Mosquea YR, Pérez-Laspiur J, Arju R, Giashuddin S, Maldonado-Martínez G, Cubano LA, Schneider RJ and Mar-

tínez-Montemayor MM. The proteome signature of the inflammatory breast cancer plasma membrane identifies novel molecular markers of disease. Am J Cancer Res 2016; 6: 1720-1740.
[22] Chen MK, Xia W, Dong Q, Du Y, Wang HL, Tapia C, Wei Y, Han Y, Chu YY, Yam C, Gao Y, Wang YH, Meric-Bernstam F, Liu J, Wang SC, Yu D and Hung MC. Abstract 5682: synergism of PARP inhibitor and MET inhibitor in multiple cancer types with intrinsic and acquired PARP inhibitor resistances. Cancer Res 2020; 80: 5682-5682.
[23] Martin M. Cutadapt removes adapter sequences from high-throughput sequencing reads. EMBnetjournal 2011; 17: 10.
[24] Patro R, Duggal G, Love MI, Irizarry RA and Kingsford C. Salmon provides fast and bias-aware quantification of transcript expression. Nat Methods 2017; 14: 417-419.
[25] Leek JT, Johnson WE, Parker HS, Jaffe AE and Storey JD. The sva package for removing batch effects and other unwanted variation in high-throughput experiments. Bioinformatics 2012; 28: 882-883.
[26] Love MI, Huber W and Anders S. Moderated estimation of fold change and dispersion for RNA-seq data with DESeq2. Genome Biol 2014; 15: 550.
[27] Hänzelmann S, Castelo R and Guinney J. GSVA: gene set variation analysis for microarray and RNA-seq data. BMC Bioinformatics 2013; 14: 7.
[28] Wu D and Smyth GK. Camera: a competitive gene set test accounting for inter-gene correlation. Nucleic Acids Res 2012; 40: e133.
[29] Ritchie ME, Phipson B, Wu D, Hu Y, Law CW, Shi W and Smyth GK. limma powers differential expression analyses for RNA-sequencing and microarray studies. Nucleic Acids Res 2015; 43: e47.
[30] Subramanian A, Tamayo P, Mootha VK, Mukherjee S, Ebert BL, Gillette MA, Paulovich A, Pomeroy SL, Golub TR, Lander ES and Mesirov JP. Gene set enrichment analysis: a knowledge-based approach for interpreting genome-wide expression profiles. Proc Natl Acad Sci U S A 2005; 102: 15545-15550.
[31] Liberzon A, Subramanian A, Pinchback R, Thorvaldsdóttir H, Tamayo P and Mesirov JP. Molecular signatures database (MSigDB) 3.0. Bioinformatics 2011; 27: 1739-1740.
[32] Liberzon A, Birger C, Thorvaldsdóttir H, Ghandi M, Mesirov JP and Tamayo P. The molecular signatures database (MSigDB) hallmark gene set collection. Cell Syst 2015; 1: 417-425.
[33] Gendoo DM, Ratanasirigulchai N, Schröder MS, Paré L, Parker JS, Prat A and Haibe-Kains B. Genefu: an R/Bioconductor package for computation of gene expression-based signatures in breast cancer. Bioinformatics 2016; 32: 1097-1099.
[34] Wickham H. ggplot2: elegant graphics for data analysis. Springer Science & Business Media; 2009.
[35] Gu Z, Eils R and Schlesner M. Complex heatmaps reveal patterns and correlations in multidimensional genomic data. Bioinformatics 2016; 32: 2847-2849.
[36] Dobin A, Davis CA, Schlesinger F, Drenkow J, Zaleski C, Jha S, Batut P, Chaisson M and Gingeras TR. STAR: ultrafast universal RNA-seq aligner. Bioinformatics 2013; 29: 15-21.
[37] Robinson JT, Thorvaldsdóttir H, Winckler W, Guttman M, Lander ES, Getz G and Mesirov JP. Integrative genomics viewer. Nat Biotechnol 2011; 29: 24-26.
[38] Subramanian A, Narayan R, Corsello SM, Peck DD, Natoli TE, Lu X, Gould J, Davis JF, Tubelli AA, Asiedu JK, Lahr DL, Hirschman JE, Liu Z, Donahue M, Julian B, Khan M, Wadden D, Smith IC, Lam D, Liberzon A, Toder C, Bagul M, Orzechowski M, Enache OM, Piccioni F, Johnson SA, Lyons NJ, Berger AH, Shamji AF, Brooks AN, Vrcic A, Flynn C, Rosains J, Takeda DY, Hu R, Davison D, Lamb J, Ardlie K, Hogstrom L, Greenside P, Gray NS, Clemons PA, Silver S, Wu X, Zhao WN, Read-Button W, Wu X, Haggarty SJ, Ronco LV, Boehm JS, Schreiber SL, Doench JG, Bittker JA, Root DE, Wong B and Golub TR. A next generation connectivity map: L1000 platform and the first 1,000,000 profiles. Cell 2017; 171: 1437-1452, e1417.
[39] Li H and Durbin R. Fast and accurate short read alignment with Burrows-Wheeler transform. Bioinformatics 2009; 25: 1754-1760.
[40] Ritz C, Baty F, Streibig JC and Gerhard D. Dose-response analysis using R. PLoS One 2015; 10: e0146021.
[41] Wang X, Spandidos A, Wang H and Seed B. PrimerBank: a PCR primer database for quantitative gene expression analysis, 2012 update. Nucleic Acids Res 2012; 40: D1144-1149.
[42] Untergasser A, Cutcutache I, Koressaar T, Ye J, Faircloth BC, Remm M and Rozen SG. Primer3--new capabilities and interfaces. Nucleic Acids Res 2012; 40: e115.
[43] Ye J, Coulouris G, Zaretskaya I, Cutcutache I, Rozen S and Madden TL. Primer-BLAST: a tool to design target-specific primers for polymerase chain reaction. BMC Bioinformatics 2012; 13: 134.
[44] Zámborszky J, Szikriszt B, Gervai JZ, Pipek O, Póti Á, Krzystanek M, Ribli D, Szalai-Gindl JM, Csabai I, Szallasi Z, Swanton C, Richardson AL and Szüts D. Loss of BRCA1 or BRCA2 markedly increases the rate of base substitution

mutagenesis and has distinct effects on genomic deletions. Oncogene 2017; 36: 746-755.
[45] Benjamini Y and Hochberg Y. Controlling the false discovery rate: a practical and powerful approach to multiple testing. J R Stat Soc Series B Stat Methodol 1995; 57: 289-300.
[46] Gogola E, Rottenberg S and Jonkers J. Resistance to PARP inhibitors: lessons from preclinical models of BRCA-associated cancer. Annu Rev Cancer Biol 2019; 3: 235-254.
[47] Hustedt N and Durocher D. The control of DNA repair by the cell cycle. Nat Cell Biol 2016; 19: 1-9.
[48] Elstrodt F, Hollestelle A, Nagel JH, Gorin M, Wasielewski M, van den Ouweland A, Merajver SD, Ethier SP and Schutte M. BRCA1 mutation analysis of 41 human breast cancer cell lines reveals three new deleterious mutants. Cancer Res 2006; 66: 41-45.
[49] Sakai W, Swisher EM, Karlan BY, Agarwal MK, Higgins J, Friedman C, Villegas E, Jacquemont C, Farrugia DJ, Couch FJ, Urban N and Taniguchi T. Secondary mutations as a mechanism of cisplatin resistance in BRCA2-mutated cancers. Nature 2008; 451: 1116-1120.
[50] Pettitt SJ, Frankum JR, Punta M, Lise S, Alexander J, Chen Y, Yap TA, Haider S, Tutt ANJ and Lord CJ. Clinical reversion analysis identifies hotspot mutations and predicted neoantigens associated with therapy resistance. Cancer Discov 2020; 10: 1475-1488.
[51] Lin KK, Harrell MI, Oza AM, Oaknin A, Ray-Coquard I, Tinker AV, Helman E, Radke MR, Say C, Vo LT, Mann E, Isaacson JD, Maloney L, O'Malley DM, Chambers SK, Kaufmann SH, Scott CL, Konecny GE, Coleman RL, Sun JX, Giordano H, Brenton JD, Harding TC, McNeish IA and Swisher EM. Reversion mutations in circulating tumor DNA predict primary and acquired resistance to the parp inhibitor rucaparib in high-grade ovarian carcinoma. Cancer Discov 2019; 9: 210-219.
[52] Weigelt B, Comino-Méndez I, de Bruijn I, Tian L, Meisel JL, García-Murillas I, Fribbens C, Cutts R, Martelotto LG, Ng CKY, Lim RS, Selenica P, Piscuoglio S, Aghajanian C, Norton L, Murali R, Hyman DM, Borsu L, Arcila ME, Konner J, Reis-Filho JS, Greenberg RA, Robson ME and Turner NC. Diverse *BRCA1* and *BRCA2* reversion mutations in circulating cell-free DNA of therapy-resistant breast or ovarian cancer. Clin Cancer Res 2017; 23: 6708-6720.
[53] Chen HD, Guo N, Song SS, Chen CH, Miao ZH and He JX. Novel mutations in intron 11 and overexpression of COX-2 and BIRC3 mediate cellular resistance to PARP inhibitors. Am J Cancer Res 2020; 10: 2813-2831.
[54] Cheng DT, Mitchell TN, Zehir A, Shah RH, Benayed R, Syed A, Chandramohan R, Liu ZY, Won HH, Scott SN, Brannon AR, O'Reilly C, Sadowska J, Casanova J, Yannes A, Hechtman JF, Yao J, Song W, Ross DS, Oultache A, Dogan S, Borsu L, Hameed M, Nafa K, Arcila ME, Ladanyi M and Berger MF. Memorial sloan kettering-integrated mutation profiling of actionable cancer targets (MSK-IMPACT): a hybridization capture-based next-generation sequencing clinical assay for solid tumor molecular oncology. J Mol Diagn 2015; 17: 251-264.
[55] Sholl LM, Do K, Shivdasani P, Cerami E, Dubuc AM, Kuo FC, Garcia EP, Jia Y, Davineni P, Abo RP, Pugh TJ, van Hummelen P, Thorner AR, Ducar M, Berger AH, Nishino M, Janeway KA, Church A, Harris M, Ritterhouse LL, Campbell JD, Rojas-Rudilla V, Ligon AH, Ramkissoon S, Cleary JM, Matulonis U, Oxnard GR, Chao R, Tassell V, Christensen J, Hahn WC, Kantoff PW, Kwiatkowski DJ, Johnson BE, Meyerson M, Garraway LA, Shapiro GI, Rollins BJ, Lindeman NI and MacConaill LE. Institutional implementation of clinical tumor profiling on an unselected cancer population. JCI Insight 2016; 1: e87062.
[56] Kwong A, Cheuk IW, Shin VY, Ho CY, Au CH, Ho DN, Wong EY, Yu SW, Chen J, Chan KK, Ngan HY, Chan TL and Ma ES. Somatic mutation profiling in-negative breast and ovarian cancer patients by multigene panel sequencing. Am J Cancer Res 2020; 10: 2919-2932.
[57] Shibue T and Weinberg RA. EMT, CSCs, and drug resistance: the mechanistic link and clinical implications. Nat Rev Clin Oncol 2017; 14: 611-629.
[58] Tokumaru Y, Oshi M, Katsuta E, Yan L, Satyananda V, Matsuhashi N, Futamura M, Akao Y, Yoshida K and Takabe K. KRAS signaling enriched triple negative breast cancer is associated with favorable tumor immune microenvironment and better survival. Am J Cancer Res 2020; 10: 897-907.
[59] Schacke M, Kumar J, Colwell N, Hermanson K, Folle GA, Nechaev S, Dhasarathy A and Lafon-Hughes L. PARP-1/2 inhibitor olaparib prevents or partially reverts EMT induced by TGF-β in NMuMG cells. Int J Mol Sci 2019; 20: 518.
[60] Murthy V, Oshi M, Tokumaru Y, Endo I and Takabe K. Increased apoptosis is associated with robust immune cell infiltration and cytolytic activity in breast cancer. Am J Cancer Res 2021; 11: 3674-3687.
[61] Oshi M, Gandhi S, Tokumaru Y, Yan L, Yamada A, Matsuyama R, Ishikawa T, Endo I and Takabe K. Conflicting roles of expression by subtypes in breast cancer. Am J Cancer Res 2021; 11: 5094-5110.
[62] Oshi M, Gandhi S, Angarita FA, Kim TH, Tokumaru Y, Yan L, Matsuyama R, Endo I and Takabe K. A novel five-gene score to predict complete pathological response to neoadjuvant

chemotherapy in ER-positive/HER2-negative breast cancer. Am J Cancer Res 2021; 11: 3611-3627.

[63] Zhang Y, Di X, Chen G, Liu J, Zhang B, Feng L, Cheng S and Wang Y. An immune-related signature that to improve prognosis prediction of breast cancer. Am J Cancer Res 2021; 11: 1267-1285.

[64] Takeshita T, Yan L, Peng X, Kimbung S, Hatschek T, Hedenfalk IA, Rashid OM and Takabe K. Transcriptomic and functional pathway features were associated with survival after pathological complete response to neoadjuvant chemotherapy in breast cancer. Am J Cancer Res 2020; 10: 2555-2569.

[65] Gutierrez Barrera AM, Fouad TM, Song J, Webster R, Elsayegh N, Wood AL, Demir A, Litton JK, Ueno NT and Arun BK. BRCA mutations in women with inflammatory breast cancer. Cancer 2018; 124: 466-474.

[66] Ibrahim YH, García-García C, Serra V, He L, Torres-Lockhart K, Prat A, Anton P, Cozar P, Guzmán M, Grueso J, Rodríguez O, Calvo MT, Aura C, Díez O, Rubio IT, Pérez J, Rodón J, Cortés J, Ellisen LW, Scaltriti M and Baselga J. PI3K inhibition impairs BRCA1/2 expression and sensitizes BRCA-proficient triple-negative breast cancer to PARP inhibition. Cancer Discov 2012; 2: 1036-1047.

Table S1. Compounds that oppose transcriptional changes in resistant clones

compound	similarity	FDR
phorbol-12-myristate-13-acetate	-0.075	1.8E-68
ingenol	-0.060	2.0E-46
pyrvinium-pamoate	-0.065	2.0E-44
IKK-2-inhibitor-V	-0.045	1.0E-22
niclosamide	-0.036	3.7E-18
prostratin	-0.080	1.2E-17
phorbol-myristate-acetate	-0.050	1.2E-16
obatoclax	-0.069	1.5E-16
kinetin-riboside	-0.039	5.2E-15
mebendazole	-0.035	1.4E-14
tyrphostin-A9	-0.050	9.9E-14
COT-10b	-0.033	4.3E-12
malonoben	-0.046	6.5E-12
KO-143	-0.037	6.5E-12
BX-795	-0.036	4.5E-11
QS-11	-0.034	1.7E-10
FCCP	-0.039	9.9E-10
heliomycin	-0.064	1.4E-09
DG-041	-0.033	2.1E-09
CCCP	-0.050	3.5E-09
tunicamycin	-0.045	6.5E-09
BRD-K99636700	-0.030	8.3E-09
quinoclamine	-0.030	9.1E-09
vinblastine	-0.031	3.0E-08
vincristine	-0.029	6.6E-07
bithionol	-0.040	9.3E-07
rhodomyrtoxin-b	-0.046	2.5E-06
BRD-K80786583	-0.044	3.7E-06
HU-211	-0.042	7.1E-06
AG-592	-0.040	8.3E-06
BRD-K20109053	-0.048	1.6E-05
selamectin	-0.037	3.1E-05
BRD-A05680309	-0.042	3.8E-05
plinabulin	-0.038	5.6E-05
tyrphostin-AG-879	-0.031	5.6E-05
helveticoside	-0.041	8.0E-05
BRD-K08448573	-0.041	2.2E-04
gitoxigenin	-0.032	3.3E-04
pyrvinium	-0.048	3.8E-04
XL-147	-0.035	3.9E-04
SA-247615	-0.031	4.2E-04
BRD-K23319301	-0.042	4.4E-04
KM-03949SC	-0.040	4.8E-04
cercosporin	-0.037	5.0E-04
BRD-K61102114	-0.069	5.4E-04
BRD-K31706415	-0.039	6.7E-04
A-23187	-0.031	9.7E-04

I-070759	-0.034	1.1E-03
BRD-K18163752	-0.034	1.1E-03
VU-0418947-2	-0.039	1.5E-03
ivermectin	-0.031	1.5E-03
morin	-0.031	1.9E-03
clofarabine	-0.031	2.0E-03
BRD-A14014306	-0.038	2.5E-03
flubendazole	-0.034	2.5E-03
BRD-K44732214	-0.038	2.7E-03
BRD-K19166598	-0.032	2.8E-03
BRD-K01614657	-0.032	3.0E-03
RJC-00245SC	-0.036	3.3E-03
VU-0418939-2	-0.037	3.4E-03
BRD-K39597586	-0.033	4.1E-03
BRD-K30231186	-0.049	5.5E-03
cinobufagin	-0.030	7.7E-03
BRD-A43805296	-0.035	7.8E-03
JTC-801	-0.042	8.9E-03
BRD-K50011261	-0.048	9.3E-03
BRD-K05197617	-0.033	9.3E-03
BRD-K83194053	-0.031	9.3E-03
phenamil	-0.031	1.2E-02
BRD-K28934562	-0.034	1.2E-02
BRD-A69429454	-0.032	1.8E-02
BRD-K55844427	-0.031	2.1E-02
BRD-K01176062	-0.075	2.5E-02
BRD-K68866125	-0.032	2.8E-02
BRD-K49712247	-0.031	3.7E-02
BRD-K98824517	-0.032	3.7E-02
oligomycin-c	-0.032	3.9E-02
BRD-K63305270	-0.071	4.2E-02
BRD-K18891555	-0.051	4.2E-02
YL-54	-0.031	4.7E-02
p-aminophenethylspiperone	-0.041	5.1E-02
vindesine	-0.031	5.8E-02
genipin	-0.031	5.9E-02
BRD-K81249055	-0.049	5.9E-02
hexachlorophene	-0.040	6.2E-02
BRD-K20718732	-0.030	6.8E-02
BRD-K23802982	-0.039	7.6E-02
BRD-K64577556	-0.066	8.4E-02
BRD-K48332509	-0.047	8.5E-02
BRD-K70489510	-0.046	9.3E-02
BRD-K71424167	-0.053	9.5E-02

Table S2. Compounds that reinforce transcriptional changes in resistant clones

compound	similarity	FDR
selumetinib	0.044	4.0E-30
PD-0325901	0.048	6.3E-29
PD-184352	0.050	2.6E-28
AS-605240	0.045	1.2E-25
AZD-8330	0.048	1.2E-17
tanespimycin	0.031	4.0E-15
trametinib	0.044	1.1E-14
ERK-inhibitor-11E	0.039	1.6E-13
PD-98059	0.033	6.3E-13
NVP-AUY922	0.030	1.6E-12
neratinib	0.030	3.3E-11
AZ-628	0.033	3.9E-10
budesonide	0.033	5.4E-10
dabrafenib	0.050	5.8E-08
AS-703026	0.047	8.0E-08
U0126	0.044	4.9E-07
PP-1	0.043	1.0E-06
MEK1-2-inhibitor	0.042	1.6E-06
PU-H71	0.043	2.6E-06
BRD-A66861218	0.036	2.1E-05
PP-2	0.034	3.2E-05
anthothecol	0.045	1.6E-04
BRD-K88707333	0.039	1.3E-03
BIIB-021	0.033	1.7E-03
hydrocortisone-valerate	0.031	2.0E-03
methylprednisolone	0.037	2.1E-03
WZ-3146	0.031	2.8E-03
BRD-K77508012	0.037	2.8E-03
MD-040	0.032	3.1E-03
halometasone	0.039	3.3E-03
CCT-018159	0.030	3.7E-03
triamcinolone-acetonide	0.033	3.9E-03
fluocinolone-acetonide	0.032	6.9E-03
BRD-K74316684	0.038	8.8E-03
BIBU-1361	0.030	1.5E-02
BRD-K98803880	0.030	2.0E-02
BRD-K92981876	0.031	2.6E-02
BRD-K69317358	0.052	3.1E-02
depomedrol	0.032	3.6E-02
BRD-K05323441	0.040	6.4E-02
5-aminolevulinic-acid	0.030	6.6E-02

Table S3. qRT-PCR primer sequences

name	sequence	gene
BRCA1-F	ACCTTGGAACTGTGAGAACTCT	*BRCA1*
BRCA1-R	TCTTGATCTCCCACACTGCAATA	*BRCA1*
TP53BP1-F	ATGGACCCTACTGGAAGTCAG	*TP53BP1*
TP53BP1-R	TTTCTTTGTGCGTCTGGAGATT	*TP53BP1*
CDK1-F	AAACTACAGGTCAAGTGGTAGCC	*CDK1*
CDK1-R	TCCTGCATAAGCACATCCTGA	*CDK1*
CHEK1-F	ATATGAAGCGTGCCGTAGACT	*CHEK1*
CHEK1-R	TGCCTATGTCTGGCTCTATTCTG	*CHEK1*
REV7-F	ACCGCCCAGTGGAGAAATTC	*MAD2L2*
REV7-R	CATCGCACACGCTGATCTT	*MAD2L2*
GAPDH-F	GGAGCGAGATCCCTCCAAAAT	*GAPDH*
GAPDH-R	GGCTGTTGTCATACTTCTCATGG	*GAPDH*
18S-F	GTAACCCGTTGAACCCCATT	*18S*
18S-R	CCATCCAATCGGTAGTAGCG	*18S*

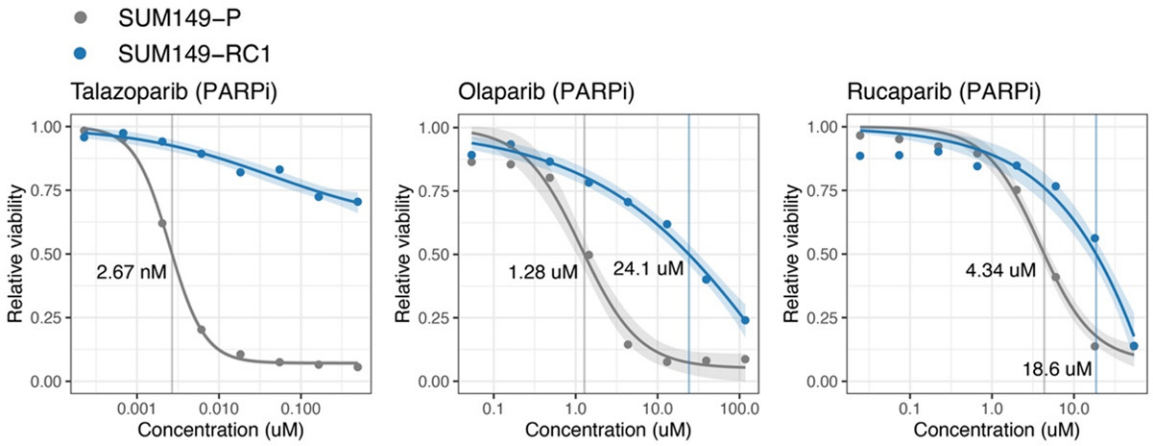

Figure S1. Drug sensitivities of PARPi-resistant and parental clones to PARP inhibitors. Cell viabilities are relative to DMSO vehicle control. IC50 values are shown whenever available.

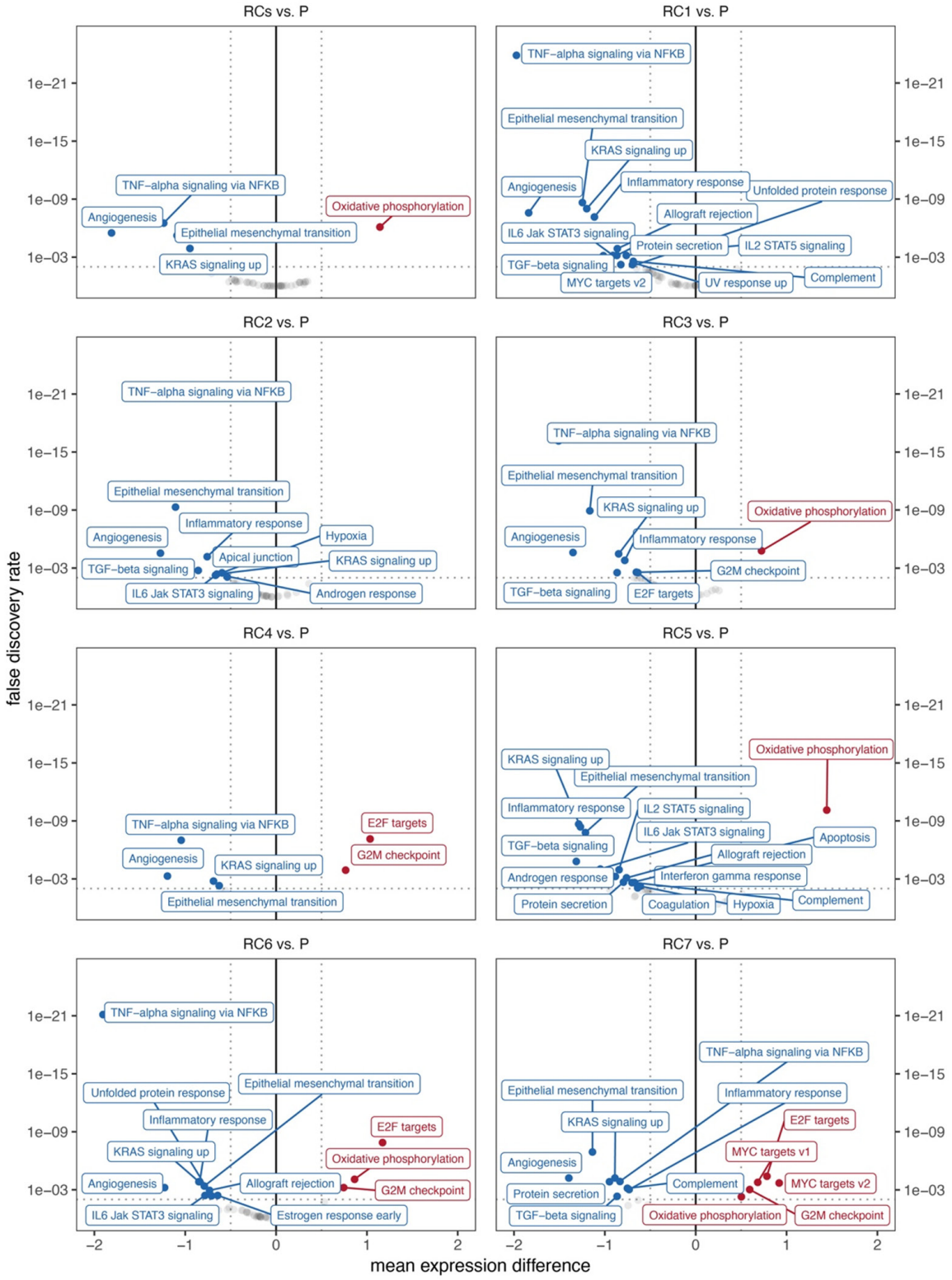

Figure S2. Upregulated and downregulated pathways in resistant clones vs. parental. Volcano plots of differential pathways by competitive analyses comparing differential gene expression statistics inside vs. outside each gene set using CAMERA.

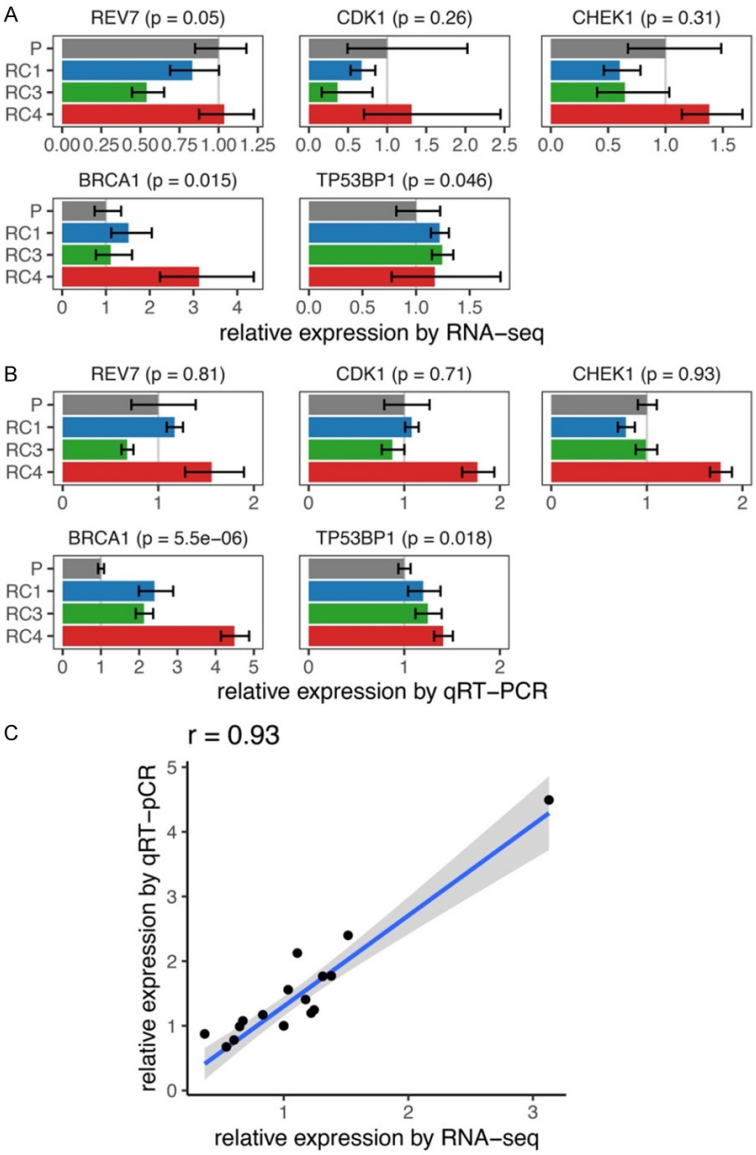

Figure S3. Comparison of RNA-seq and qRT-PCR expression levels of selected genes. A. Differential expressions by RNA-seq, relative to the parental clone, across 3 biological replicates. Error bars represent 80% confidence intervals. Significance of the difference compared to the parental clone was assesed by the t-test. B. Differential expression by qRT-PCR, across duplicates across 2 independent experiments, assessed by the t-test. Error bars represent 80% confidence intervals. C. Correlation between qRT-PCR and RNA-seq relative expression measurements.

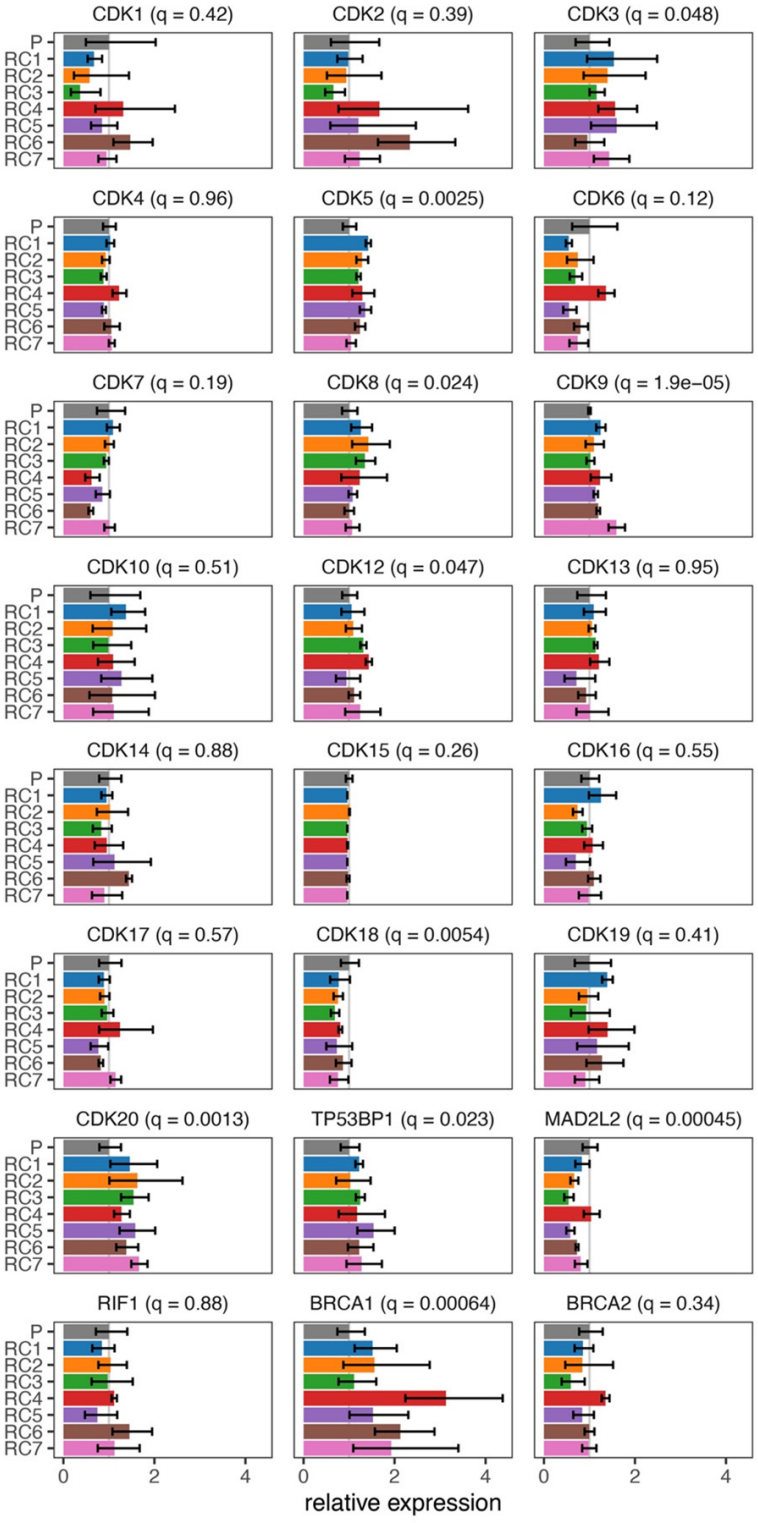

Figure S4. Expression levels of cyclin-dependent kinases and DNA repair genes. Bars represent relative expression levels (as measured by RNA-seq) compared to the parental clone. Error bars span 80% confidence intervals across 3 biological replicates. Displayed q-values represent the significances of the expression differences between all resistant clones vs. the parental clone, as assessed by the t-test and corrected for multiple hypothesis testing by the Benjamini-Hochberg method.

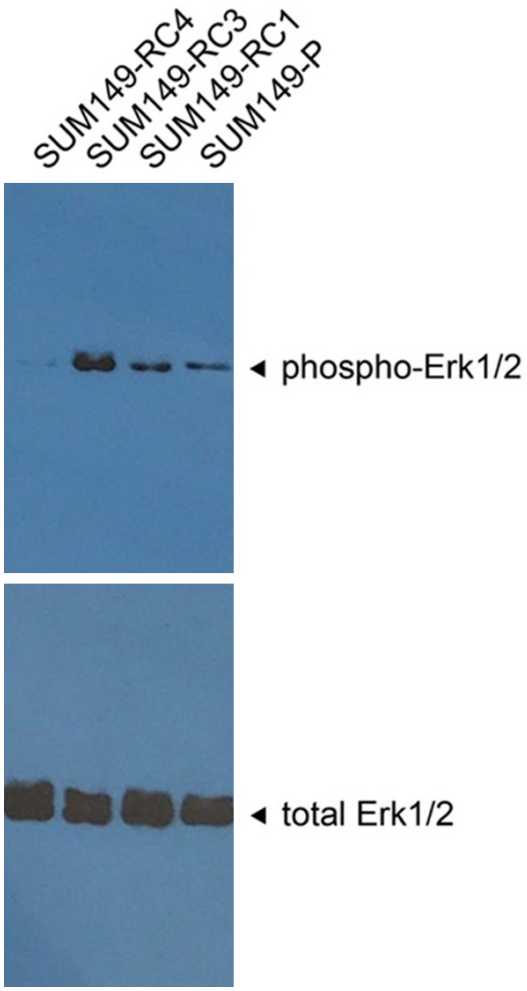

Figure S5. Western blots of phospho-ERK and total ERK levels in PARPi-resistant and parental clones.

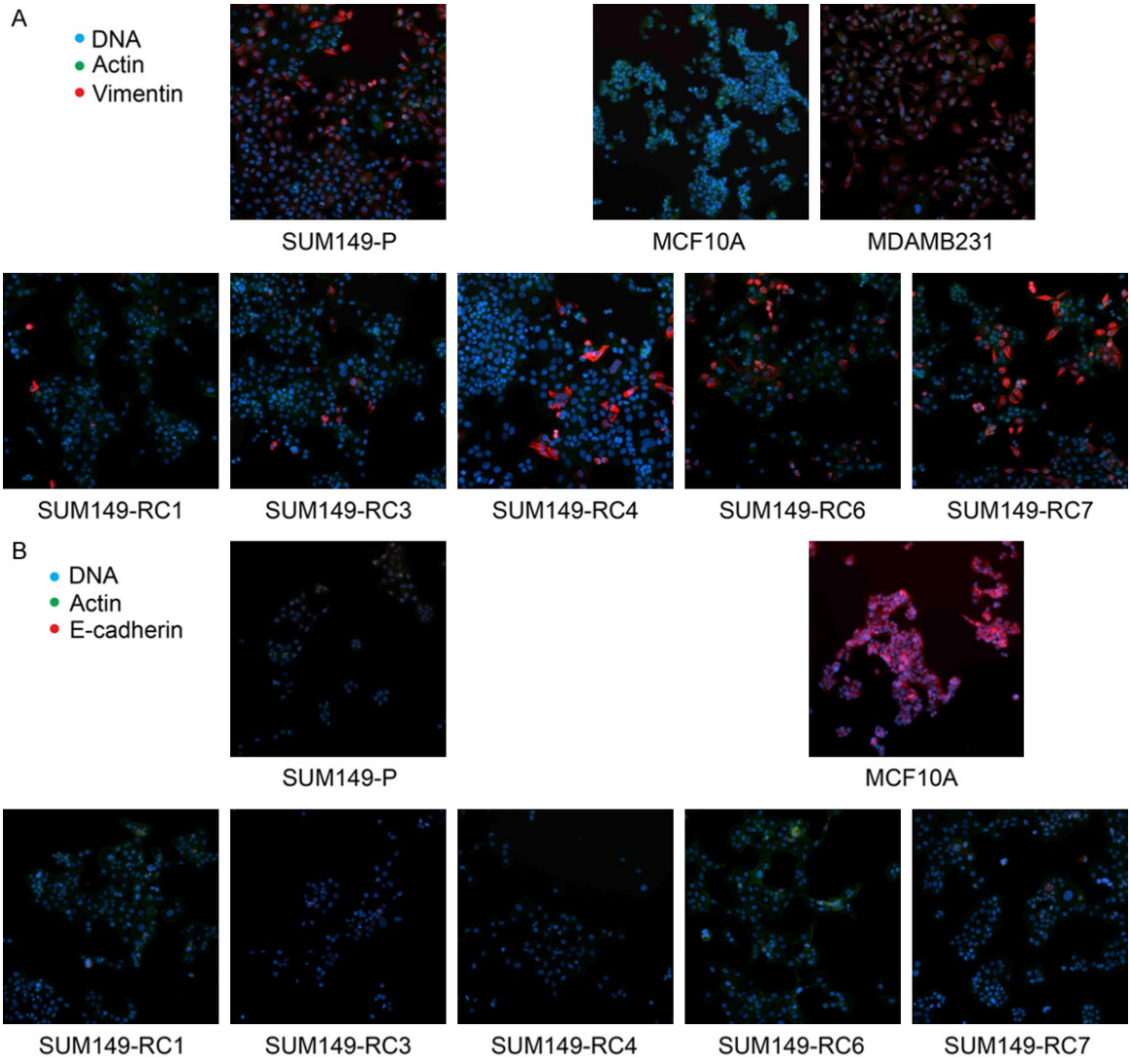

Figure S6. Immunofluorescence of MCF10A (epithelial) and MDAMB231 (mesenchymal) cells, parental SUM149 cells, and PARPi-resistant cells, staining for DNA (Hoechst), actin (phalloidin), and vimentin (A) or E-cadherin (B). Shown images are representative of 3 independent experiments. RC, PARPi-resistant clone. P, parental clone.

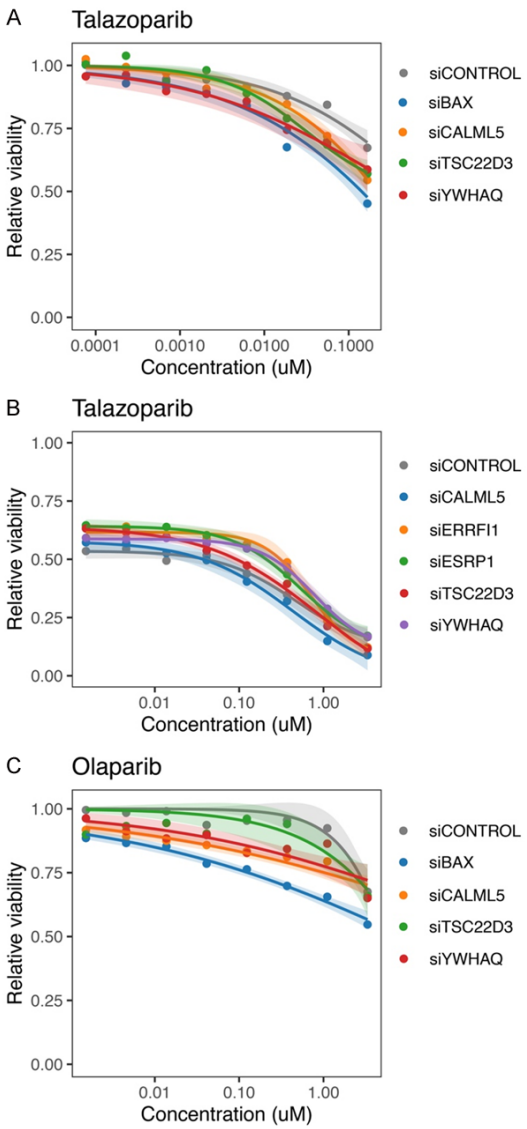

Figure S7. PARPi sensitivities of PARPi-resistant clone SUM149-RC2 after siRNA knockdown of BAX, CALML5, ERRFI1, ESRP1, TSC22D3, or YWHAQ. Cell viabilities are relative to DMSO vehicle control. A. Sensitivities to talazoparib. B. Sensitivities to high concentrations of talazoparib. C. Sensitivities to olaparib.

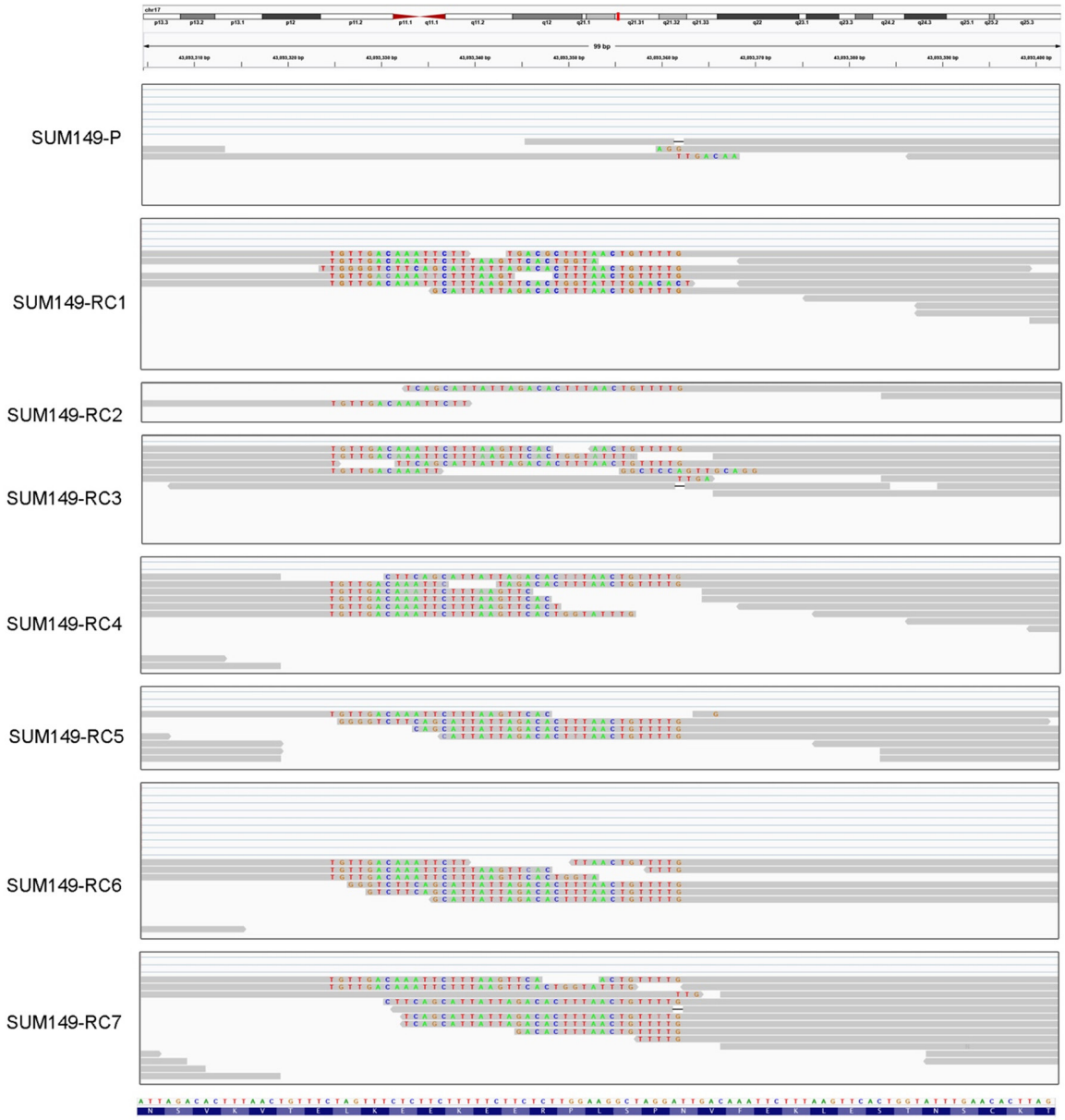

Figure S8. RNA-seq reads mapping to *BRCA1* exon 10 in parental and resistant clones. Reads are visualized using the Integrative Genomics Viewer with soft-clipped bases shown.

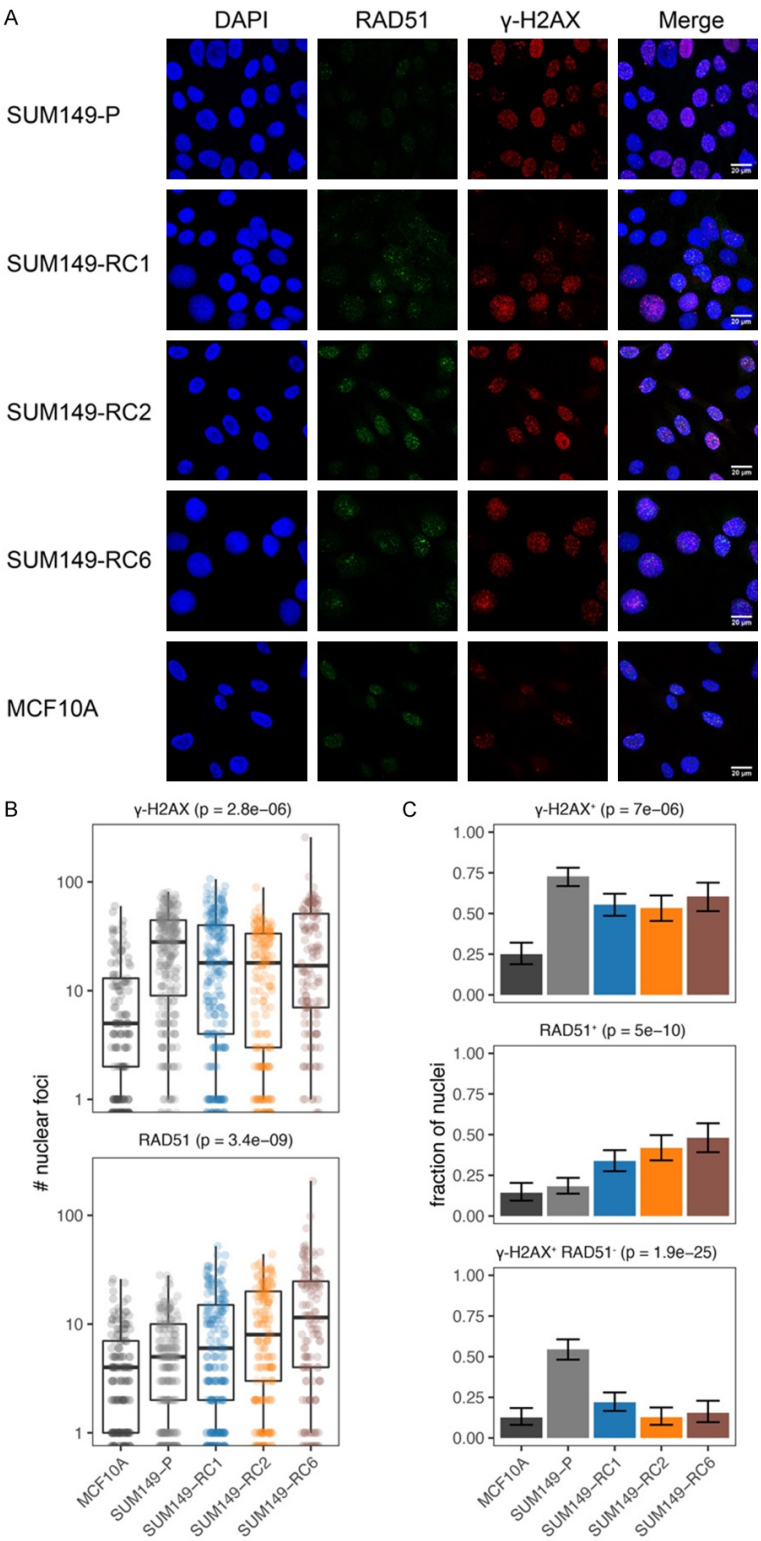

Figure S9. Restoration of homologous repair in PARPi-resistant *BRCA1*-revertant clones. A. Immunofluorescence of MCF10A (BRCA1/2 wildtype), SUM149-P (*BRCA1* mutant), and PARPi-resistant clones (*BRCA1* revertant), staining for DAPI (DNA), RAD51 (homologous repair), and γ-H2AX (double-strand breaks) after 24 h of 50 nM talazoparib treatment. B. Quantification of the number of nuclear foci in each sample. C. Fractions of nuclei that are positive for γ-H2AX foci or RAD51 foci, where positivity is defined as ≥10 foci. Resistant clones are collectively compared against the parental clone by the Fisher's exact test.

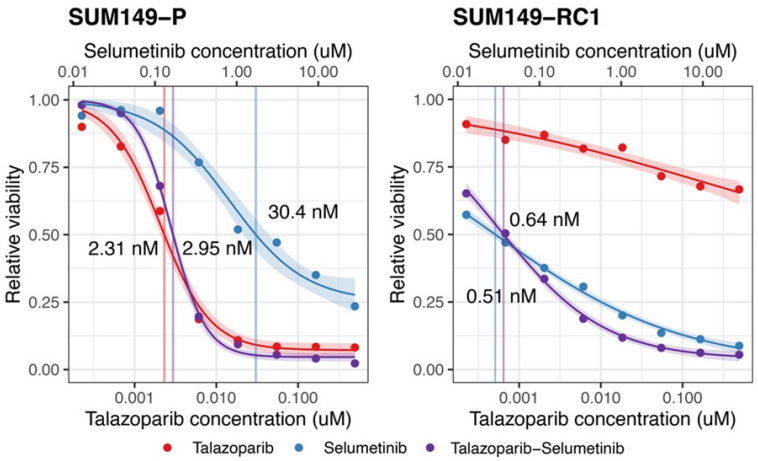

Figure S10. Sensitivities of PARPi-resistant and parental clones to talazoparib, selumetinib, or a concurrent combination thereof. Cell viabilities are relative to DMSO vehicle control. IC50 values are shown whenever available.

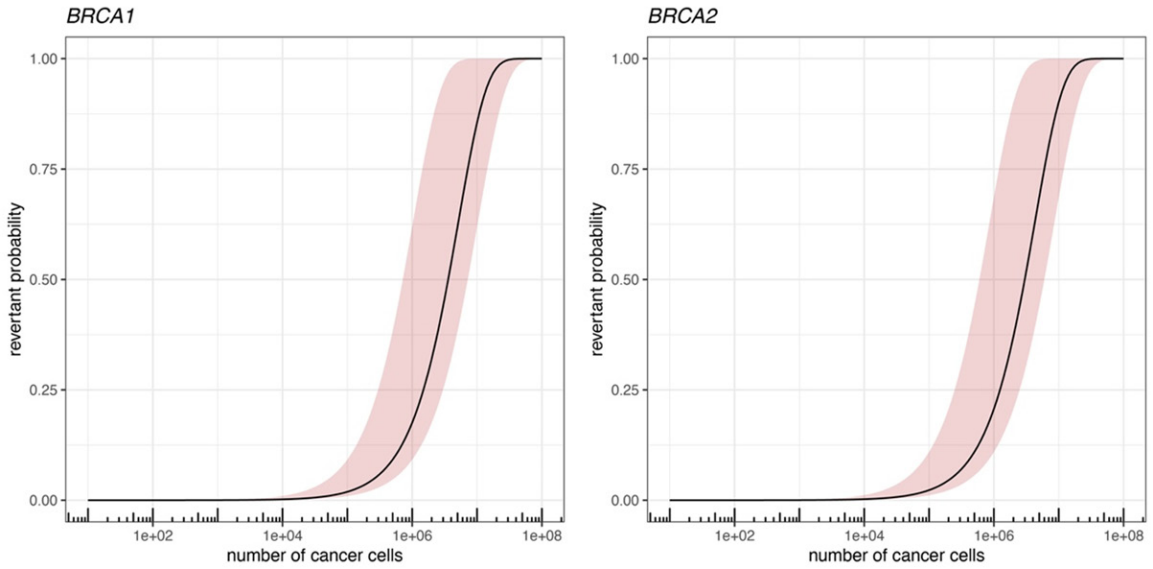

Figure S11. Probability of revertant mutations in *BRCA1* and *BRCA2*. The probability that at least one revertant cell emerges from a population of *BRCA1* or *BRCA2*-/- mutants (harbouring a 1 bp frameshift deletion) is estimated based on the frequency of 1 bp insertions reported in *BRCA1* or *BRCA2*-/- mutants. The revertant mutation must land within 20 codons of the original mutation, with a range of 10 to 100 codons (red confidence band).